
1 **Robustness-The sensitivity of simulatingsimulated aerosol climatic **impacts****
2 **impact to domain size using regional model: ~~the sensitivity to domain size~~**
3 **(WRF-Chem v3.6)**

4 ¹Xiaodong Wang, ^{1,2,3}Chun Zhao*, ¹Mingyue Xu, ¹Qiuyan Du, ¹Jianqiu Zheng, ¹Yun Bi,
5 ¹Shengfu Lin, ⁴Yali Luo

6
7
8 ¹School of Earth and Space Sciences, University of Science and Technology of China, Hefei,
9 China

10 ²CAS Center for Excellence in Comparative Planetology, University of Science and Technol
11 ogy of China, Hefei, China

12 ³Frontiers Science Center for Planetary Exploration and Emerging Technologies, University
13 of Science and Technology of China, Hefei, China

14
15 ⁴State Key Laboratory of Severe Weather, Chinese Academy of Meteorological Sciences,
16 Beijing, China

17
18
19
20 Manuscript for submission to *Geoscientific Model Development*

21
22
23
24 *Corresponding authors: Chun Zhao (chunzhao@ustc.edu.cn)

25
26
27
28 **Key points:**

- 29 1. Domain size has a great influence on the simulated meteorological fields and aerosol
30 distribution during East Asian summer monsoon (EASM).
31 2. Regional simulations with different domain sizes demonstrate consistently that aerosols
32 weaken EASM moisture transport.
33 3. Different domain sizes result in different strength of aerosol-induced changes of temperature
34 and thus circulation and rainfall over China.

35
36
37

38 Abstract

39 Domain size can have significant ~~impacts~~impact on regional modeling results, but few
40 studies ~~examining~~examined the sensitivities of ~~regional modeling results of simulated~~
41 ~~impacts~~impact to regional domain size. This study investigates the regional modeling
42 sensitivities of aerosol ~~impacts~~impact on East Asian summer monsoon (EASM) to domain size.
43 The simulations with two different domain sizes demonstrate consistently that aerosols induce
44 the cooling of lower-t-troposphere that leads to the anti-cyclone circulation anomalies and thus
45 the weakening of EASM moisture transport. The aerosol-induced adjustment of monsoonal
46 circulation results in ~~a spatial an alternate increase and decrease~~ pattern of “~~+++~~” ~~for~~
47 precipitation-~~change~~ over the continent of China. Domain size has a great influence on the
48 simulated meteorological fields. For example, the simulation with ~~increasing~~larger domain size
49 produces weaker EASM circulation, which also ~~affect~~affects aerosol distributions significantly.
50 This leads to the difference of simulated strength and area extent of aerosol-induced changes
51 of lower-tropospheric temperature and pressure, which further results in different
52 ~~locations~~distributions of circulation and precipitation anomalies over the continent of China.
53 For example, over Southeast China, aerosols induce the increase (decrease) of precipitation
54 from the smaller-domain (larger-domain) simulation. Different domain sizes simulate
55 consistently aerosol-induced increase of precipitation around 30°N over East China. This study
56 highlights the important ~~impacts~~influence of domain size on regional modeling results of
57 aerosol ~~impacts~~impact on circulation and precipitation, which may not be limited to East Asia.
58 More generally, this study also implies that proper modeling of meteorological fields with
59 appropriate domain size is one of the keys to simulate robust aerosol climatic ~~impacts~~impact.

60

61

62

63

64

65

66

67 1. Introduction

68 As one of the forcing's of climate change, aerosol contributes the largest uncertainty to
69 the total radiative forcing estimate, and it has attracted more and more attention since the 1980s
70 (IPCC, 2013; Li et al., 2019). ~~Aerosols~~Aerosol can absorb and scatter solar radiation through
71 ~~Aerosol Radiation~~aerosol-radiation interactions, affect the regional radiation budget, and
72 amplify its impact through atmospheric mixing and circulation (e.g., Schwartz, 1996; Rinke et
73 al., 2004; Kim et al., 2007; Z. Q. Li et al., 2010; ~~C.~~ Zhao et al., 2011, 2012, 2014; Myhre et al.,
74 2013; Kuniyal et al., 2019; Zhang et al., 2020). Serving as cloud condensation nuclei or ice
75 nuclei, ~~aerosols~~aerosol can change the microscopic and macroscopic characteristics of clouds
76 and affect the climate, which is called ~~Aerosol-Cloud~~aerosol-cloud interactions (Twomey,
77 1977; Albrecht, 1989; Ackerman et al., 2000; Fan et al., 2012, 2013, 2016). ~~And there~~There
78 are ~~many also some~~ other possible ~~Aerosol-Cloud-Precipitation processes which~~aerosol-cloud-
79 precipitation interactions that may amplify or dampen this effect (Rosenfeld et al., 2008, 2014;
80 Tao et al., 2012; Fan et al., 2015, 2018).

81 Due to the large population and the rapid economic development in last few decades,
82 East Asia has encountered large aerosol loading, and suffered from severe air pollution caused
83 by various emission sources (e.g., Chan et al., 2008; X. Y. Zhang et al., 2012; Li et al., 2017;
84 An et al., 2019). Moreover, East Asia is ~~located in~~within the monsoon region, ~~the and its~~
85 weather and climate systems are more complicated, which makes the ~~study~~studying of aerosol
86 effects more challenging (Ding et al., 2005; Ding, 2007; Li et al., 2016, 2019; Wu et al., 2016).
87 In recent decades, the East Asian summer monsoon (EASM) and ~~summer~~the associated
88 precipitation in eastern China have shown strong ~~interdecadal~~inter-decadal changes (Ding et
89 al., 2008, 2013; Zhou et al., 2009; Zhu et al., 2011; Zhang, 2015), which ~~had~~has a significant
90 impact on agriculture, economy, and human life (An et al., 2015). Many factors ~~are~~may be
91 related to the ~~interdecadal~~inter-decadal variability of the EASM, such as extraterrestrial natural
92 forcing, internal dynamical feedbacks within the climate system, and changes in atmospheric
93 composition (e.g., greenhouse gases and aerosols) and surface conditions (land cover
94 ~~changes~~change or urbanization) related to anthropogenic factors (Ding et al., 2008, 2009; H.
95 M. Li et al., 2010; Song ~~&~~and Zhou, 2014; Xiao ~~&~~and Duan, 2016; Jiang et al., 2017). As one
96 of the forcing factors ~~of summer climate change in East Asia~~, aerosol ~~have~~has attracted many
97 people to study ~~theirs effect on~~ weather and climate ~~effects of summer aerosols in of~~ East Asia
98 (Cowan ~~&~~and Cai, 2011; H. Zhang et al., 2012; Guo et al., 2013; Jiang et al., 2013, 2017; Wu

99 et al., 2013; Song et al., 2014; Li et al., 2015, 2018; Wang et al., 2015, 2017; Chen et al., 2016;
100 Kim et al., 2016; Xie et al., 2016; Dong et al., 2019).

101 Numerous studies have used global climate models to study the ~~impacts~~impact of
102 anthropogenic ~~aerosols~~aerosol on the EASM climate and understand the mechanisms
103 underneath (e.g., Guo et al., 2013; Jiang et al., 2013, 2017; Song et al., 2014; Yan et al., 2015;
104 Chen et al., 2016; Wang et al., 2017; Li et al., 2018; Dong et al., 2019). The global modeling
105 results have shown that ~~aerosols tend~~aerosol tends to reduce the land-sea thermal contrast,
106 weaken the EASM, and thereby reduce the rainfall over the continent (e.g., Guo et al., 2013;
107 Jiang et al., 2013; Song et al., 2014; Wang et al., 2017; Li et al., 2018; Dong et al., 2019). The
108 reduction of monsoon precipitation over the continent may reduce the release of latent heat
109 from condensation in the upper troposphere and further weaken the ~~East-Asian summer~~
110 ~~monsoon~~EASM (e.g., Jiang et al., 2013; Li et al., 2019). Jiang et al. (2013) used the CAM5
111 (the Community Atmospheric Model version 5) model to study the effect of different aerosol
112 types on ~~East-Asian summer~~ clouds and precipitation during the EASM, and found that all
113 anthropogenic aerosols suppressed the precipitation in North China and enhanced the
114 precipitation in South China and the adjacent ocean areas. Through analyzing the CMIP5
115 (Coupled Model Intercomparison Program phase 5) modeling results, Song et al. (2014)
116 examined the contributions of different ~~forcings~~forcing's (aerosol forcing, greenhouse gas
117 forcing, and natural forcing) to the weakening of EASM circulation during 1958–2001, and
118 They found that aerosol forcing playsplayed a major role ~~in the weakening of EASM, and the~~
119 ~~contribution of natural forcing is almost negligible, and the forcing of greenhouse gases is~~
120 ~~conducive to slightly strengthening rather than weakening the monsoon circulation.~~

121 Global climate models have been widely used for investigating aerosol ~~impacts~~;
122 ~~however~~impact. However, there are still large uncertainties with the results at regional scale,
123 partly because the regional-scale monsoon rainband and aerosol distributions are still not able
124 to be described accurately with relatively lower model horizontal resolution (H. ~~M~~-Li et al.,
125 2010; Guo et al., 2013; Jiang et al., 2013; Song et al., 2014; Li et al., 2018; Dong et al., 2019).
126 In comparison, regional model often has relatively higher horizontal resolution and can better
127 capture regional features of weather and climate systems and aerosol distributions, and
128 therefore has been used to investigate aerosol regional climatic ~~impacts~~impact recently (e.g.,
129 Zhang et al., 2009; Stanelle et al., 2010; Zhao et al., 2011, 2012; Wu et al., 2013; Wang et al.,
130 2015; Crippa et all, 2017; Zhuang et al., 2018). For example, usingCrippa et al. (2017) found
131 that the enhanced resolution (from 60 to 12 km) can improve the regional model performance
132 of meteorological fields and aerosol optical depth (AOD). Using the regional model

133 (RegCCMS), Wang et al. (2015) found that aerosol-cloud interaction ~~decreases~~decreased the
134 ~~autoconversion~~auto-conversion rates of cloud water to rain water and ~~increases~~increased the
135 liquid water path of clouds in East China, ~~strengthens~~which further strengthened the cooling
136 of lower atmosphere caused by ~~the direct aerosol~~-radiation ~~effect~~interaction and
137 ~~suppresses~~suppressed the convective precipitation. Wu et al. (2013), with the regional model
138 (WRF-Chem), found that the aerosol heating effect caused the cloud to move northward over
139 East China and led to the increased precipitation in the north.

140 Although regional model at higher horizontal resolution may better capture regional
141 features of wind, cloud, precipitation, and aerosol, it also introduces additional uncertainties
142 on modeling regional aerosol climatic ~~impacts~~impact resulted from the lateral boundary
143 conditions of regional simulation. Previous studies have found that domain size of regional
144 model ~~can~~could significantly influence the simulation results (e.g., Warner et al., 1997; Leduc
145 and Laprise, 2009; Leduc et al., 2011; Bhaskaran et al., 2012; Diaconescu et al., 2013; Di Luca
146 et al., 2015; Giorgi, 2019). For example, Bhaskaran et al. (2012) studied the sensitivity of ~~the~~
147 simulated hydrological cycle to the regional domain size over the Indian subcontinent. They
148 found that the simulations with smaller domains produced the increased precipitation and
149 evapotranspiration on seasonal mean and the higher number of moderate precipitation days
150 relative to the ones with larger domains. Different distributions of cloud, precipitation, and
151 winds from the simulations with different domain sizes may lead to different aerosol
152 distributions and ~~its~~the associated climatic ~~impacts~~impact. Previous studies have found that
153 aerosol ~~impacts~~impact on precipitation, clouds, and circulation ~~will~~would be significantly
154 different under different weather and climate conditions (e.g., Wu et al., 2013; Wang et al.,
155 2015; Xie et al., 2016). In addition, Seth and Giorgi. (1998) found that the smaller-domain
156 simulation produced better precipitation compared with the observations, but resulted in an
157 unrealistic response to the internal forcing. This indicates that the simulation domain size may
158 also affect the aerosol ~~impacts~~impact on large-scale circulation. Therefore, the regional
159 simulation with increased domain size may be preferred to ~~better~~-reflect the overall aerosol
160 ~~impacts~~impact on large-scale circulation and ~~weather~~climate system without ~~the~~-strict
161 constraint from ~~the~~ boundary forcing (e.g., Seth and Giorgi, 1998; Leduc and Laprise, 2009;
162 Xue et al., 2014), but the increased domain size may make the ~~simulation~~simulation deviated
163 from the forcing such as the reanalysis.

164 As far as we know, there are few studies examining the sensitivities of regional
165 modeling results of aerosol ~~impacts~~impact to ~~regional~~-domain size. Although it can be expected
166 that domain size will play a role, it is ~~not known~~unknown to what extent and how domain size

167 can affect modeling results of aerosol climatic [impacts](#). Therefore, in this study, the
168 regional online-coupled meteorology and chemistry model WRF-Chem (Weather Research
169 and Forecasting model coupled with Chemistry) (Grell et al., 2005; Skamarock et al., 2008) is
170 used to study the aerosol [impacts](#) on ~~East-Asian-summer-monsoon~~the EASM system
171 ~~and~~with the focus on the modeling sensitivities to regional domain size. WRF-Chem has been
172 widely used for studying aerosol meteorological and climatic [impacts](#) over East Asia
173 (e.g.,A. J. Ding et al., 2013; Wu et al., 2013; Gao et al., 2014; Chen et al., 2014; Zhao et al.,
174 2014; Huang et al., 2016; Liu et al., 2016; Petaja et al., 2016; Zhao B et al., 2017). The
175 investigation of aerosol [impacts](#) under different simulated meteorological fields due to
176 different domain sizes may also help understand the different modeling results about the
177 aerosol [impacts](#) on ~~East-Asian-summer-monsoon~~EASM from previous studies. The
178 study is organized as follows. Section 2 describes the numerical experiments and methods. The
179 results and discussions are presented in Section 3. A summary is provided in Section 4.

180

181 2. Methodology

182 2.1 WRF-Chem

183 In this study, the version of WRF-Chem updated by the University of Science and
184 Technology of China (USTC version of WRF-Chem) is used. The model simulates the
185 emission, transport, mixing, and chemical transformation of trace gases and aerosols
186 simultaneously with the meteorology, and can be used for investigation of regional-scale air
187 quality and interactions between meteorology and chemistry. Compared with the publicly
188 released version, the USTC version of WRF-Chem includes a few additional functions, such
189 as the diagnosis of radiative forcing of aerosol species, optimized Kain-Fritsch (KF) convection
190 scheme, aerosol-snow interaction, land surface coupled biogenic Volatile Organic Compound
191 (VOC) emission, etc. (Zhao et al., 2013a, b, 2014, 2016; Hu et al., 2019; Du et al., 2020), all
192 of which may have important impact on modeling aerosol and its climatic [impacts](#).

193 The Model for Simulating Aerosol Interactions and Chemistry (MOSAIC) aerosol
194 module coupled with CBM-Z (carbon bond mechanism) photochemical mechanism in WRF-
195 Chem is selected in this study (Zaveri & Peters, 1999; Zaveri et al., 2008). MOSAIC uses a
196 sectional approach to represent aerosol size distributions with four or eight discrete size bins
197 in the current version of WRF-Chem (Fast et al., 2006). To reduce the computational cost, four
198 discrete size bins is selected in this study. All major aerosol components including sulfate,
199 nitrate, ammonium, black carbon, organic matter, sea-salt, mineral dust, and other inorganic

200 matter (OIN) are simulated in the model. The MOSAIC aerosol scheme includes physical and
201 chemical processes of nucleation, condensation, coagulation, aqueous-phase chemistry, and
202 water uptake by aerosols. Dry deposition of aerosol mass and number is simulated following
203 the approach of Binkowski and Shankar (1995), which includes both turbulent diffusion and
204 gravitational settling. Wet removal of aerosols by grid-resolved stratiform clouds and
205 precipitation includes in-cloud removal (rainout) and below-cloud removal (washout) by
206 impaction and interception, following Easter et al. (2004) and Chapman et al. (2009). In this
207 study, cloud-ice-borne aerosols are not explicitly treated in the model, but the removal of
208 aerosols by the droplet freezing process is considered. Convective transport and wet removal
209 of aerosols by cumulus clouds is coupled with the Kain-Fritsch cumulus scheme as Zhao et al.
210 (2013b). Aerosol radiative feedback is coupled with the Rapid Radiative Transfer Model
211 (RRTMG) (Mlawer et al., 1997; Iacono et al., 2000) for both SW and LW radiation as
212 implemented by Zhao et al. (2011). The optical properties and direct radiative forcing of
213 individual aerosol species in the atmosphere are diagnosed following the methodology
214 described in Zhao et al. (2013a).

215

216 2.2 Numerical experiments

217 Four sets of experiments, CTRL-L, CTRL-S, CLEAN-L, and CLEAN-S, with different
218 simulation domain sizes or emission configurations are conducted as explained and listed in
219 Table 1. The control experiments (CTRL-S, and CTRL-L) ~~simulations~~ use standard
220 anthropogenic emission dataset (described in Section 2.3), while the clean simulations
221 (CLEAN-S, and CLEAN-L) apply a factor of 0.1 on the standard emissions within the small
222 domain to represent a clean atmosphere condition over East Asia (Fig. 1). The CTRL-L and
223 CTRL-S (CLEAN-L and CLEAN-S) represent the simulations with large and small domain
224 sizes, respectively, as shown in FigureFig. 1. The aerosol ~~impacts~~impact can be calculated by
225 the difference between the CTRL and CLEAN simulations for each simulation domain. The
226 comparison of aerosol ~~impacts between the large and small simulation domains implies the~~
227 ~~sensitivity of aerosol impacts to domain size.~~impact between the large and small simulation
228 domains implies the sensitivity of aerosol impact to domain size. Besides these experiments,
229 another set of experiment NoRA-S is conducted to isolate aerosol-radiation and aerosol-cloud
230 interactions for further understanding the mechanisms of aerosol impact, which is also listed
231 in Table 1. The horizontal resolution of 30 km is selected for both simulation domains with the
232 consideration of the balance of computational efficiency and modeling performance,
233 particularly for the larger domain. The comparable horizontal resolutions have also been

widely used for investigating aerosol impact on regional climate (e.g., Zhang et al., 2009; Stanelle et al., 2010; Zhao et al., 2011, 2012; Chen et al., 2014; Wang et al., 2015).

All the WRF-Chem experiments select the Morrison two-moment microphysics (Morrison et al., 2009), Kain-Fritsch cumulus scheme (Kain, 2004), unified Noah land-surface model, Rapid Radiative Transfer Model (RRTMG) longwave and shortwave radiation schemes (Iacono et al., 2008), and MYNN planetary boundary layer (PBL) scheme (Nakanishi & Niino, 2006, 2009). Following Du et al. (2020), the PBL mixing coefficient is modified to simulate better PBL mixing of aerosols. Five ensemble simulations are performed for each experiment by changing the simulation initial condition time at UTC 0000 from May ~~12~~¹²th to May ~~16~~¹⁶th, 2017. (i.e., the five ensemble simulations start at UTC 0000 of May 12th, 13th, 14th, 15th, and 16th, respectively). The averaged results from five ensembles are analyzed to reduce the influence of modeling internal variability. The simulations run continuously through entire June and July of 2017. The analysis focuses on the simulation results for June 1 to July 31, 2017. The meteorological initial and lateral boundary conditions are derived from National Centers for Environmental Prediction (NCEP) Final (FNL) Operational Global Analysis data (NCEP, 2000) with a horizontal resolution of $1^{\circ} \times 1^{\circ}$ and a ~~time~~temporal resolution of 6h. The chemical initial and boundary conditions are provided by a quasi-global WRF-Chem simulation for the same time period. The quasi-global WRF-Chem simulation is performed at $1^{\circ} \times 1^{\circ}$ horizontal resolution with 360×130 grid cells (180°W - 180°E , 60°S - 70°N). More details about the general configuration of a quasi-global WRF-Chem simulation can be found in Zhao et al. (2013b) and Hu et al. (2016). The simulation configuration is summarized in Table 2.

2.3 Emissions

Biomass burning emissions are obtained from the Fire Inventory (FINN) of the National Center for Atmospheric Research with hourly temporal resolution and 1 km horizontal resolution (Wiedinmyer et al., 2011), and the injection heights follow Dentener et al. (2006) for the Aerosol Comparison between Observations and Models (AeroCom) project. The natural dust emission fluxes are calculated based on the adjusted GOCART dust emission scheme (Ginoux et al., 2001; Zhao et al., 2010), and the emitted dust particles are distributed into the MOSAIC aerosol size bins following a theoretical expression based on the physics of scale-invariant fragmentation of brittle materials derived by Kok (2011). More details about the dust emission scheme coupled with MOSAIC aerosol scheme in WRF-Chem can be found in Zhao et al. (2010, 2013b). Sea-salt emission follows Zhao et al. (2013a), which includes the

correction of particles with radius less than 0.2 μm and the dependence of sea-salt emission on sea surface temperature. Anthropogenic emissions are obtained from the Multi-resolution Emission Inventory for China (MEIC) at $0.1^\circ \times 0.1^\circ$ horizontal resolution and with monthly temporal resolution for 2015 (Li et al., 2017; Zheng et al., 2018), except that the emissions outside of China are from the Hemispheric Transport of Air Pollution version2 (HTAPv2) at $0.1^\circ \times 0.1^\circ$ horizontal resolution and with monthly temporal resolution for the year 2010 (Janssens-Maenhout et al., 2015) (Fig. 1). As discussed above, the anthropogenic ~~emission~~emission in the CLEAN experiments ~~is~~has a factor of 0.1 of that in the CTRL experiment, ~~and~~. In addition, in the CLEAN-L experiment, only the emissions in the area of ~~the~~ small domain (denoted by the red box) are adjusted. In this way, the emission reduction from the simulations with both domains are made consistent.

2.4 Observations and reanalysis

Although the aims of this study are not evaluating the simulation results to determine the optimal model configuration for the experiments, some observations and reanalysis datasets are still used to provide the references for the key fields. The comparison with these references can demonstrate whether the simulation results are acceptable for further analysis. The MISR (Multi-angle Imaging SpectroRadiometer, instrument on board the NASA Terra platform) retrieval dataset is used as a reference of spatial distribution of AOD (Diner et al, 1998; Martonchik et al., 2004). When showing the comparison between the MISR retrieved and the simulated AOD, the simulation results are sampled from 10 am - 11 am for averaging and at the locations of the retrievals because the Terra platform passes over the equator at about 10:45 LT (Diner et al, 2001). The precipitation datasets of CMA (National Meteorological Information Center of China Meteorological Administration) and CMORPH (Climate Prediction Center MORPHing technique) are used as the references for spatial and temporal variations of precipitation during the simulation period. The CMORPH dataset is a global precipitation reanalysis dataset that is derived from geostationary satellite IR imagery (Joyce et al., 2004). The CMA rainfall was measured by tipping buckets, self-recording siphon rain gauges, or automatic rain gauges and was subject to strict quality control. The European Centre for Medium-Range Weather Forecasts (ECMWF) Reanalysis v5 (ERA5) are used as a reference for wind fields (Hersbach, 2020).

3. Results

3.1 Sensitivity of simulated meteorological fields to domain size

Figure 2 shows the spatial distributions of precipitation and moisture transport at 700 hPa over the small domain averaged for June and July of 2017 from the observation and reanalysis, and the simulations of CLEAN-S and CLEAN-L. The observation and reanalysis show that the southwesterly transports large amount of moisture into East China. The converge of large amount of moisture results in heavy precipitation over southern China and its adjacent ocean. Due to the gradual weakening of northeastward moisture transport and the blocking effect of ~~the~~ western mountains, precipitation becomes much weaker over northern and western China. Compared with the CMORPH observation and ERA5 reanalysis (Fig. 2), CLEAN-S can reasonably produce the spatial ~~distribution~~distributions of precipitation and moisture transport at 700 hPa, with slight underestimation of meridional moisture transport over eastern China. It is evident that the meridional moisture transport over southern China becomes weaker with the increasing domain size, and the eastward transport becomes stronger. In addition, the overall southwesterly moisture transport ~~shift~~shifts to the east. This leads to a decrease of precipitation over eastern China and an increase over the East China Sea. Compared with the observations of hourly precipitation from the CMA stations over eastern China (Fig. S1 in the supporting material), both the CLEAN-S and CLEAN-L experiments can generally reproduce the daily variation of precipitation over eastern China, although the CLEAN-L simulated precipitation is lower consistent with its weaker moisture transport over the region.

The difference in moisture transport between the simulations with different domain sizes results from their difference in geopotential height and wind circulation. Figure 3 shows the spatial distributions of geopotential height (GPH) and wind field at 700 hPa from the ERA5 reanalysis and the CLEAN-S simulation, and of the difference between CLEAN-L and CLEAN-S. The comparison with the ERA5 reanalysis shows that the CLEAN-S can well simulate the distributions of GPH and wind fields at 700 hPa (~~Fig. S2 in the supporting material~~). The spatial distribution of wind fields is generally consistent with that of moisture transport (Fig. 2) and is largely controlled by the West Pacific sub-tropical high (WPSH). Compared to CLEAN-S, CLEAN-L simulates lower GPH at 700 hPa and produces an anomalous lower pressure center on the East China Sea, which indicates the weaker WPSH with increasing domain size. This causes the southwestward wind anomalies over the continent, which weakens the monsoon driven northeastward moisture transport. Over the South China Sea, the westerly anomalies enhance the eastward transport of moisture.

The impact of domain size is not only on the horizontal distribution of wind fields but also on the vertical circulation. Figure 4 shows the cross-section of meridional temperature

335 anomalies and wind averaged for 105°E and 122°E from the ERA5 reanalysis and the CLEAN-
336 S simulation during June to July, and of the difference of temperature (not meridional
337 temperature anomalies) and wind between CLEAN-L and CLEAN-S. The meridional
338 temperature anomalies are calculated by subtracting the mean temperature in this latitude range
339 (as shown in Fig. 4) at each pressure level. First of all, CLEAN-S can ~~general~~generally
340 reproduce the temperature gradient and wind circulation from the ERA5 reanalysis (~~Fig. S3 in~~
341 ~~the supporting material~~). Relatively large meridional temperature gradient exists between 700
342 hPa and 200 hPa, where the temperature is higher over the South. Below 700 hPa, the
343 temperature gradient is relatively weaker, and the temperature is higher over the North. Along
344 with this distribution of temperature gradient, meridional wind blows from the South and the
345 North and converges at the latitude around 34°N, which generates strong upward motion in the
346 area of 20°N-35°N. This is consistent with the spatial ~~distribution~~distributions of precipitation
347 and moisture transport (Fig. 2). Compared with the CLEAN-S experiment, the CLEAN-L
348 experiment produces larger meridional temperature gradient between 700 hPa and 200 hPa and
349 weaker gradient below 850 hPa. The circulation from ~~the~~ CLEAN-L is generally consistent
350 with CLEAN-S, but the southerly wind from CLEAN-L is weaker and the northerly wind is
351 stronger. This results in an overall northerly wind anomalies from CLEAN-L compared with
352 CLEAN-S, and also along with a southward shift of ~~the~~ wind convergence from 34°N to 32°N.
353 It is also noteworthy that the upward motion is weakened around 22°N-38°N and strengthened
354 to the south of 20°N due to the increased domain size.

355

356 3.2 Sensitivity of simulated aerosol characteristics to domain size

357 Figure 5 shows the spatial ~~distribution~~distributions of AOD averaged for June and July
358 of 2017 from the CTRL-S simulation, and of the difference between CTRL-L and CTRL-S. ~~It~~
359 ~~can be seen that relatively~~Relatively high AOD (>0.6) exists in the Sichuan Basin and the North
360 China ~~Plain. The plain~~. AOD over East Central China and South China is relatively lower (0.2-
361 0.5), which is in line with previous ~~research~~ (studies (e.g., Luo et al., 2014; Qi et al., 2013)). In
362 general, ~~the~~ CTRL-S generally captures the spatial distribution of retrieved AOD from MISR
363 (Fig. S4S2 in the supporting material). Compared with the CTRL-S experiment, CTRL-L
364 simulates a similar spatial pattern of AOD ~~as CTRL-S~~, but produces higher AOD in southern
365 China and lower AOD in most areas of northern China. To explore the reasons of difference
366 between the two simulations, Figure 6 shows the spatial distributions of column integrated ~~total~~
367 PM_{2.5} concentration and water content in aerosol averaged ~~for~~in June and July of 2017
368 ~~from the CTRL-S simulation, and~~and of the difference between CTRL-L and CTRL-S. The

CTRL-S simulation shows high PM_{2.5} mass loading over the North China ~~Plain~~, which is consistent with the spatial distribution of AOD (Fig. 5). The PM_{2.5} mass loading also shows high values over Northwest China, which is not shown in the spatial distribution of AOD. This is mainly due to the high mass loading of dust over Northwest China (Fig. ~~S5S3~~ in the supporting material) and the water content associated with dust is relatively small.

CTRL-L simulates higher PM_{2.5} mass loading over Southeast China and lower values over North China, which is consistent with AOD. The difference of water content in aerosol shows a similar pattern. The analysis shows that the difference of PM_{2.5} mass loading over North China is mainly due to the difference of dust, while the difference over Southeast China is due to anthropogenic aerosols (Fig. ~~S5S3~~). The reduction of dust mass loading over North China from CTRL-L is primarily due to its weakening of westerlies over Northwest China compared to CTRL-S (Fig. 3), which results in less transport of dust into the downwind region. The increase of aerosol mass loading over Southeast China in CTRL-L is partly due to its less wet scavenging associated with weak precipitation (Fig. 2). The weakening of northward transport of aerosol (Fig. 3) also contributes to the increase of PM_{2.5} mass loading over southern China in CTRL-L. Besides the change of dry aerosol mass loading, the change of water content in aerosol between the two experiments also contributes to the change in AOD, which results from the difference of both dry aerosol mass and moisture.

Figure 7 shows the latitude-height cross-section of total PM_{2.5} averaged between 105°E and 122°E for June and July of 2017 from the CTRL-S experiment, and of the difference between CTRL-L and CTRL-S. The latitudinal distribution of aerosol is consistent with ~~its~~ spatial pattern with high aerosol mass concentration over North China. The mass concentration gradually reduces from the surface to the free atmosphere. The mass concentration around 500 hPa over North China can reach 5 ug/m³ that is comparable to the surface concentration over South China. In general, CTRL-L simulates higher aerosol mass concentration over South China and lower aerosol mass concentration over North China from the surface to about 500 hPa. At 32°N-36°N, CTRL-L simulates lower aerosol mass concentration near the surface and higher ~~above-values between 700 hPa and 850 hPa,~~ likely due to the difference in aerosol wet scavenging and transport between the two experiments. The difference ~~of aerosol in~~ horizontal and vertical distributions of aerosols and also the circulation patterns between the two experiments may lead to the difference in simulating aerosol ~~impacts on East Asian monsoon system~~ impact on EASM.

3.3 Sensitivity of aerosol impact to domain size

403 Before studying the sensitivity of aerosol ~~impacts~~impact to domain size, the
404 ~~impacts~~impact of aerosol on precipitation and circulation from the small domain ~~simulations~~
405 ~~are~~experiments ~~is~~ first investigated. Figure 8 shows the spatial distributions of aerosol-induced
406 difference (CTRL-CLEAN) of precipitation and moisture transport at 700 hPa averaged for
407 June and July of 2017 from the small domain simulations. The dominant effect is that aerosol
408 weakens the southwesterlies ~~flow~~ and reduces the moisture transport over the continent of
409 Central and South China (primarily between 105°E-115°E). Along the coast of Southeast China,
410 the moisture transport is enhanced slightly. Over the continent of China, aerosol induces a ~~“+-~~
411 ~~+-”~~pattern ~~an alternate increase and decrease pattern (denoted as “+-+-”)~~ of precipitation
412 changes, i.e., precipitation increases in the south of 25°N, north of 40°N, and around 30°N,
413 while decreases at 25°N~30°N and 32°N~40°N. This weakening of monsoonal circulation at
414 the lower troposphere is found mainly due to the cooling of lower troposphere and thus the
415 increase of surface pressure by aerosols (Fig. 9). The temperature averaged for lower-~~tr~~
416 troposphere (below 500 hPa) is reduced by aerosols over the continent of China, which results
417 in a positive pressure anomaly center in Southwest China. This leads to an anticyclone anomaly
418 as shown in Fig. 8, which weakens the monsoonal southwesterlies between 105°E-115°E.

419 In order to further understand the mechanisms of aerosol ~~impacts~~impact and isolate
420 aerosol-radiation and aerosol-cloud interactions, another set of numerical experiment (NoRA-
421 S) with the small domain ~~are~~is conducted, similar as CTRL-S but with the aerosol-radiation
422 interaction turned off. The difference of results between NoRA-S and CLEAN-S (NoRA-S
423 minus CLEAN-S) is interpreted as the ~~impacts~~impact of aerosol-cloud interaction, while the
424 difference of results between CTRL-S and NoRA-S (CTRL-S minus NoRA-S) is interpreted
425 as the ~~impacts~~impact of aerosol-radiation ~~interactions~~interaction. Figure 10 shows the spatial
426 ~~distribution~~distributions of the ~~impacts~~impact of aerosol-cloud and aerosol-radiation
427 interactions on (a, d) tropospheric temperature averaged below 500 hPa, (b, e) surface pressure,
428 (c, f) precipitation and moisture transport. The aerosol-cloud interaction reduces significantly
429 the lower-~~tr~~ tropospheric temperature (Fig. 10a) over a large area of South China (to the south
430 of 32°N) mainly due to its increasing of cloud amounts (Fig. ~~S6a~~S4a in the supporting material)
431 over this area, which results in an increase of surface pressure in this area (Fig. 10b). Similarly,
432 aerosol-cloud interaction also increases cloud amounts over Northeast China and its adjacent
433 ocean (Fig. ~~S6a~~S4a) and thus reduces the lower-~~tr~~ tropospheric temperature and increases the
434 surface pressure over the area. -The surface pressure over the Yellow River Basin is reduced
435 slightly by aerosol-cloud interaction, which may be due to the reduction of cloud amounts (Fig.
436 ~~S6a~~S4a) and the increase of lower-~~tr~~ tropospheric temperature. Although, the experiments can

437 generally demonstrate that aerosol-cloud interaction can largely affect cloud amount, lower-
438 tropospheric temperature, and surface pressure, please note that the co-locations of the changes
439 of cloud, temperature, and surface pressure may not be simply straightforward. For example,
440 in a fully coupled system, the cloud change due to aerosols would also adjust the temperature
441 through the release of latent heat in the atmosphere. In addition, the change of temperature
442 would also modulate the circulation and further feedback to the distributions of cloud and
443 temperature. The difference between NoRA-S and CLEAN-S over Northwest China is due to
444 the dust-radiation interaction that is included in CLEAN-S but not in NoRA-S. The analysis of
445 this study focuses on the impactsimpact of anthropogenic aerosol. The combined effect of two
446 anti-cyclone anomalies due to the two positive pressure anomalies at the lower-troposphere
447 results in the southward wind anomalies over the ocean and the northward wind anomalies over
448 North China, while the changes of circulations in other areas of China is negligible.

449 The primary impactsimpact of aerosol-radiation interaction on lower-atmospheric
450 temperature areis the positive temperature anomaliesanomaly over the Yellow Ocean and over
451 central China and the negative temperature anomaliesanomaly over the Yellow River Basin
452 and Southwest China, which is the combined effecteffect from the aerosol cooling and heating
453 at the surface and heating in the atmosphere, respectively, and also the adjustment of cloud
454 distributions (Fig. S6bS4b and Fig. S7S5). The two positive temperature anomaly centers lead
455 to two negative pressure anomaly centers and thus a large cyclone circulation anomaly over
456 the continent of East China. Therefore, it can be noted that the influence of aerosol-cloud and
457 aerosol-radiation interactions on monsoonal circulations areis counteracted over the ocean and
458 over northern China, which results in relatively small changes of monsoonal circulation over
459 the ocean and over northern China (Fig. 8). The overall aerosol impact is shown as the
460 weakening of the monsoonal circulation over the continent of central and southern China (Fig.
461 8), which is mainly contributed by the aerosol-radiation interaction.

462 Figure 11 shows the latitude-pressure cross-section of aerosol-induced difference
463 (CTRL-CLEAN) of temperature and wind averaged between 105°E and 122°E for June and
464 July of 2017 from the small domain simulation. ~~It can be seen that the~~The pattern of
465 precipitation change corresponds well to the changeschange of wind circulation. The
466 weakening of monsoonal southwesterlies resultresults in a sinking airflow anomaly around
467 28°N and the compensating upward anomaly around 24°N in the south of China, and also a
468 downdraft around 35°N and an updraft around 40°N in north China. These two sinking airflows
469 correspondscorrespond to the reduced precipitation between 25°N and 30°N and between 32°N
470 and 40°N, respectively (Fig. 8), while these updrafts correspond to the increasing precipitation

471 between 22°N and 25°N and between 32°N and 40°N. There is also weak upward
472 compensating airflow around 30°N, leading to the slight increase of precipitation in the area
473 (Fig. 8). It is noteworthy that aerosols lead to an abnormal cooling center around 33°N between
474 400 hPa to 200 hPa. This is mainly because of less solar radiation entering the atmosphere due
475 to aerosol-radiation and aerosol-cloud interactions, and also weaker monsoonal airflow that
476 leads to less release of latent heat from cloud and precipitation (Fig. S8S6 in the supporting
477 material). This cooling anomaly center also strengthens the downdraft anomalies on its both
478 sides, further weakening the monsoonal circulation.

479 In order to explore the sensitivity of aerosol ~~impacts~~impact to domain size, similar as
480 Fig. 8, Figure 12 shows the results from the large domain simulations. One consistent signal
481 between the simulations with different domain sizes is that aerosols weaken the southwesterlies
482 ~~flow~~ and reduce the moisture transport over the continent of Central and South China. The
483 difference is that this weakening is not only over the inland of China but also extending to over
484 the South China Ocean. The weakening of monsoon airflow is broader with the increasing
485 domain size, which may be due to its weaker monsoon airflow (Fig. 3) and less constraint from
486 the lateral ~~boundaries~~boundary conditions in the large domain simulation. Another consistent
487 signal between the two sets of simulations with different domain sizes is that aerosol induces
488 a similar “+--+” pattern of precipitation changes over the domain, except that the areas with
489 precipitation reduction become broader. This leads to the precipitation reduction over almost
490 the entire region between 20°N~40°N over the continent of China except the area around 30°N
491 with increasing precipitation. The increases of precipitation on the two sides of precipitation
492 reduction area shift southward to the South China ocean and northward to the north of 40°N,
493 respectively.

494 Similar as the small domain simulation, the weakening of monsoonal airflow in the
495 large domain simulation is also due to the abnormal positive lower-level pressure that is caused
496 by the lower ~~atmosphere-tropospheric~~ cooling (Fig. 13), which can also be explained by the
497 effects of aerosol-radiation and aerosol-cloud interactions (Fig. S9S7 and Fig. S10S8 in the
498 supporting material). However, compared with the small domain simulation (Fig. 9), the
499 cooling anomaly of lower-tropospheric temperature and thus the positive anomaly of lower-
500 level pressure ~~cover~~covers a broader area from the large domain simulation. The two aerosol-
501 induced cooling centers over the continent of China lead to two positive lower-level pressure
502 anomaly centers that ~~results~~result in a large anti-cycle circulation anomaly (Fig. 12), which
503 weakens the monsoonal southwesterly airflow over South China and the South China Ocean
504 and also slightly enhances the southwesterly over West China. Again, the pattern of

precipitation change corresponds well to the ~~changes~~change of wind circulation (Fig. 14). With larger domain size, aerosols lead to a broader area (between 20°N~40°N) of abnormal cooling in the troposphere up to 200 hPa. The single cooling center in the small domain simulation is split into two centers, one around 30°N at 250 hPa and another around 36°N at 700 hPa. The weakening of ~~the~~background circulation and broader cooling area lead to the broader sinking ~~airflows~~airflow over the region, which results in the broader area of reduced precipitation compared with the small domain simulation (Fig. 8 and Fig. 12). The increasing precipitation around 30°N is also resulted from the compensating ~~updrafts~~supdraft around 30°N.

4. Summary and Discussion

Due to the importance of domain size on regional modeling results and few studies ~~examining that~~ examined the sensitivities of regional modeling results of aerosol ~~impacts~~impact to domain size, this study applies the WRF-Chem model to simulate the anthropogenic aerosol ~~impacts~~impact on ~~East Asian summer monsoon~~EASM circulation and precipitation, focusing on the modeling sensitivities to regional domain size. The ~~impacts~~influence of domain size on meteorological fields, aerosol characteristics, and aerosol ~~impacts are~~impact is investigated.

First of all, the domain size has a great influence on the simulated meteorological fields. From the ~~small~~smaller domain simulation, the circulation and precipitation are in good agreement with the reanalysis data and observations. The ~~large~~larger domain simulation produces weaker ~~East Asian summer monsoon system and southward~~shifting ~~southward~~EASM ~~system~~, which results in ~~that~~ the precipitation ~~decreased~~decreases in southern China and ~~increase~~increases in the adjacent ocean. The changes of circulation and precipitation also lead to the increase of aerosol mass loading in southern China and the decrease in northern China in the ~~large~~larger domain simulation. The deviation of atmospheric fields particularly the circulation between the simulations with different domains is partly due to their different constraint from lateral boundary conditions. With ~~the~~ less constraint of ~~the~~boundary forcing ~~from~~, the ~~reanalysis data, the large~~larger domain simulation may produce negative bias in precipitation over the Yangtze River Basin and positive bias in ~~water vapor~~moisture transport over the South China Ocean as ~~reported by~~ previous studies. The uncertainties in moisture transport prescribed in the lateral ~~boundaries~~boundary conditions from the reanalysis over a larger domain may also contribute to the biases (e.g., Wang and Yang, 2008; Huang and Gao, 2018). ~~With~~Previous studies found that, with the larger ~~domain, the~~simulation ~~includes larger~~ ~~area~~domain including more areas of ocean. ~~Without, without~~ considering the ~~online~~ interaction

538 between the atmosphere and the ocean (i.e., with prescribed SST from the reanalysis), the
539 artificial positive feedback between precipitation and surface latent heat flux may overestimate
540 the precipitation over the subtropical Western North Pacific (WNP) and inhibit the westward
541 expansion of the WNP subtropical high (e.g., Cha and Lee, 2009; Lee and Cha, 2020).

542 In terms of the climatic ~~impacts~~impact of anthropogenic aerosols on ~~East Asian summer~~
543 ~~monsoon~~EASM, as shown in the schematic ~~plot~~figure (Fig. 15), aerosols induce the cooling of
544 lower troposphere over the continent through aerosol-radiation and aerosol-cloud interactions,
545 which leads to an increase of regional pressure at lower atmosphere. The regional positive
546 pressure anomalies result in the anti-cyclone circulation anomalies and thus ~~weakens~~weaken
547 the summer monsoonal northeastward moisture transport, which is consistent with previous
548 studies (e.g., Y. Q. Jiang et al., 2013; Song et al., 2014; T. J. Wang et al., 2015; Xie et al.,
549 2016). The weakening of monsoonal circulation leads to several sinking airflows and
550 compensating updrafts that correspond well to the regions with the decrease and increase of
551 precipitation, respectively, showing a spatial pattern of “+--+” for precipitation change. The
552 difference in ~~the aerosol impacts~~impact from the numerical experiments with different domain
553 sizes is mainly determined by their simulated different strength and area extent of the aerosol-
554 induced lower-tropospheric negative temperature anomalies. Compared with the smaller-
555 domain simulation, the larger-domain simulation with weaker monsoonal circulation generates
556 a broader area with negative temperature and positive pressure anomalies at the lower
557 troposphere, which results in broader sinking airflows and thus broader areas of precipitation
558 reduction over the continent of China. This could lead to the opposite signals of precipitation
559 change due to aerosols over China, ~~for~~ For example, over Southeast China, the ~~increase and~~
560 ~~decrease of~~ precipitation is increased (decreased) from the smaller-domain ~~and~~ (larger-domain
561 ~~simulations, respectively.)~~ simulation. The consistent signal of aerosol ~~impacts~~impact between
562 the simulations with different domain sizes is the increasing precipitation around 30°N that is
563 resulted from the compensating updraft over the region.

564 Although the modeling results of aerosol ~~impacts~~impact in this study may have some
565 uncertainties associated with physical and chemical processes, emissions, and ~~simulation~~
566 horizontal resolutions, (e.g., Di Luca et al., 2015; Crippa et al., 2019), it highlights the
567 ~~impacts~~impact of simulation domain size on regional modeling aerosol ~~impacts~~impact on
568 monsoonal circulation and precipitation, which may not be limited to the region of East Asia.
569 Uncertainties of modeling aerosol climatic ~~impacts~~impact are often investigated ~~focusing with~~
570 the focus on aerosol characteristics such as their distributions and properties. This study adds
571 another complexity (impact of domain size) on regional modeling of aerosol climatic

572 ~~impacts~~impact. More specifically, ~~although on one hand~~, larger-domain simulation may better
573 allow ~~aerosol~~ feedbacks ~~of aerosol impacts~~ on weather and climate systems without strong
574 lateral boundary constraint (e.g., Seth and Giorgi, 1998; Leduc and Laprise, 2009); ~~Diaconescu~~
575 ~~et al., 2013~~), but it may produce biased meteorological fields compared to smaller-domain
576 simulation, which can ~~then~~ significantly influence the modeling results of aerosol
577 ~~impacts~~impact. On the other hand, although the simulation with smaller domain produces
578 ~~better large-scale circulation compared to the reanalysis, the lateral boundary condition may~~
579 ~~also have stronger constraint on aerosol feedbacks to large-scale circulation. Therefore, not~~
580 ~~like meteorological fields or aerosol properties, there is no direct observation or reanalysis that~~
581 ~~can be used as the references to evaluate aerosol impact (Di Luca et al., 2015; Crippa et al.,~~
582 ~~2017), and the optimal configuration of simulation domain is hard to be determined in this~~
583 ~~study~~. It may be the key to ~~simulate reasonable/less biased~~improve the simulated
584 meteorological fields with larger regional domain or global domain in order to model robust
585 aerosol climatic ~~impacts~~impact. More generally, this study also highlights the ~~impacts~~impact
586 of background meteorological fields (without aerosol effect) on simulated aerosol
587 ~~impacts~~impact. Proper modeling of background meteorological fields is one of the keys to
588 simulate ~~robust~~reliable aerosol climatic ~~impacts~~impact. The model inter-comparison study of
589 aerosol climatic ~~impacts~~impact should also focus on the diversity of simulated background
590 meteorological fields besides aerosol characteristics.

593 **Data statement**

594 **Code and data availability**

595 The release version of WRF-Chem can be downloaded from
596 http://www2.mmm.ucar.edu/wrf/users/download/get_source.html. The code of updated
597 USTC version of WRF-Chem is available at <https://doi.org/10.5281/zenodo.4663508> or
598 contact ~~chunzhao@ustc.edu.cn~~chunzhao@ustc.edu.cn. ~~The dataset from the European~~
599 ~~Centre for Medium-Range Weather Forecasts (ECMWF) Reanalysis v5 (ERA5) can be~~
600 ~~downloaded from https://rda.ucar.edu/datasets/ds633.1/ (last access: Aug 2021). The~~
601 ~~CMORPH data can be downloaded from~~
602 ~~https://ftp.cpc.ncep.noaa.gov/precip/CMORPH_V1.0/CRT/0.25deg-DLY_00Z/2017/ (last~~
603 ~~access: Aug 2021).~~

605 **Author contributions**

606 Xiaodong Wang and Chun Zhao designed the experiments, conducted and analyzed the
607 simulations. All authors contributed to the discussion and final version of the paper.

608

609 **Acknowledgements**

610 This research was supported by the [National Basic Research Program of China \(Grant](#)
611 [2018YFC1507400\)](#), National Natural Science Foundation of China (42061134009, 41775146,
612 91837310), the USTC Research Funds of the Double First-Class Initiative (YD2080002007),
613 Fundamental Research Funds for the Central Universities (WK2080000101), and the Strategic
614 Priority Research Program of Chinese Academy of Sciences (XDB41000000). The study used
615 the computing resources from the High-Performance Computing Center of University of
616 Science and Technology of China (USTC) and the TH-2 of National Supercomputer Center in
617 Guangzhou (NSCC-GZ).

618

619

620 **Reference**

- 621 Ackerman, A. S., Toon, O. B., Stevens, D. E., Heymsfield, A. J., Ramanathan, V., & Welton,
622 E. J. (2000). Reduction of tropical cloudiness by soot. *Science*, **288**(5468), 1042-1047.
623 <https://doi.org/10.1126/science.288.5468.1042>
- 624 Albrecht, B. A. (1989). Aerosols, Cloud Microphysics, and Fractional Cloudiness. *Science*,
625 **245**(4923), 1227-1230. <https://doi.org/10.1126/science.245.4923.1227>
- 626 An, Z. S., Wu, G. X., Li, J. P., Sun, Y. B., Liu, Y. M., Zhou, W. J., et al. (2015). Global
627 Monsoon Dynamics and Climate Change. *Annual Review of Earth and Planetary*
628 *Sciences*, **43**, 29-77. <https://doi.org/10.1146/annurev-earth-060313-054623>
- 629 An, Z. S., Huang, R. J., Zhang, R. Y., Tie, X. X., Li, G. H., Cao, J. J., et al. (2019). Severe haze
630 in northern China: A synergy of anthropogenic emissions and atmospheric processes.
631 *Proceedings of the National Academy of Sciences of the United States of America*,
632 **116**(18), 8657-8666. <https://doi.org/10.1073/pnas.1900125116>
- 633 Bhaskaran, B., Ramachandran, A., Jones, R., & Moufouma-Okia, W. (2012). Regional climate
634 model applications on sub-regional scales over the Indian monsoon region: The role of
635 domain size on downscaling uncertainty. *Journal of Geophysical Research-*
636 *Atmospheres*, **117**. <https://doi.org/10.1029/2012jd017956>
- 637 Binkowski, F. S., & Shankar, U. (1995). The Regional Particulate Matter Model .1. Model
638 description and preliminary results. *Journal of Geophysical Research-Atmospheres*,
639 **100**(D12), 26191-26209. <https://doi.org/10.1029/95jd02093>
- 640 Carvalho, D., Rocha, A., Gomez-Gesteira, M., & Santos, C. S. (2014). WRF wind simulation
641 and wind energy production estimates forced by different reanalyses: Comparison with
642 observed data for Portugal. *Applied Energy*, **117**, 116-126.
643 <https://doi.org/10.1016/j.apenergy.2013.12.001>
- 644 Cha, D. H., & Lee, D. K. (2009). Reduction of systematic errors in regional climate simulations
645 of the summer monsoon over East Asia and the western North Pacific by applying the
646 spectral nudging technique. *Journal of Geophysical Research-Atmospheres*, **114**.
647 <https://doi.org/10.1029/2008jd011176>
- 648 Chan, C. K., & Yao, X. (2008). Air pollution in mega cities in China. *Atmospheric Environment*,
649 **42**(1), 1-42. <https://doi.org/10.1016/j.atmosenv.2007.09.003>
- 650 Chapman, E. G., Gustafson, W. I., Easter, R. C., Barnard, J. C., Ghan, S. J., Pekour, M. S., &
651 Fast, J. D. (2009). Coupling aerosol-cloud-radiative processes in the WRF-Chem model:

652 Investigating the radiative impact of elevated point sources. *Atmospheric Chemistry*
653 *and Physics*, **9**(3), 945-964. <https://doi.org/10.5194/acp-9-945-2009>

654 Chen, S. Y., Zhao, C., Qian, Y., Leung, L. R., Huang, J. P., Huang, Z. W., et al. (2014).
655 Regional modeling of dust mass balance and radiative forcing over East Asia using
656 WRF-Chem. *Aeolian Research*, **15**, 15-30.
657 <https://doi.org/10.1016/j.aeolia.2014.02.001>

658 Chen, J. P., Chen, I. J., & Tsai, I. C. (2016). Dynamic Feedback of Aerosol Effects on the East
659 Asian Summer Monsoon. *Journal of Climate*, **29**(17), 6137-6149.
660 <https://doi.org/10.1175/Jcli-D-15-0758.1>

661 Colin, J., Deque, M., Radu, R., & Somot, S. (2010). Sensitivity study of heavy precipitation in
662 Limited Area Model climate simulations: influence of the size of the domain and the
663 use of the spectral nudging technique. *Tellus Series a-Dynamic Meteorology and*
664 *Oceanography*, **62**(5), 591-604. <https://doi.org/10.1111/j.1600-0870.2010.00467.x>

665 Cowan, T., & Cai, W. (2011). The impact of Asian and non-Asian anthropogenic aerosols on
666 20th century Asian summer monsoon. *Geophysical Research Letters*, **38**.
667 <https://doi.org/10.1029/2011gl047268><https://doi.org/10.1029/2011gl047268>.

668 [Crippa, P., Sullivan, R. C., Thota, A., and Pryor, S. C.: The impact of resolution on](#)
669 [meteorological, chemical and aerosol properties in regional simulations with WRF-](#)
670 [Chem, Atmos. Chem. Phys., 17, 1511–1528, https://doi.org/10.5194/acp-17-1511-](#)
671 [2017, 2017.](#)

672 [Crippa, P., Sullivan, R. C., Thota, A., & Pryor, S. C. \(2019\). Sensitivity of simulated aerosol](#)
673 [properties over eastern North America to WRF-Chem parameterizations. Journal of](#)
674 [Geophysical Research: Atmospheres, 124, 3365–3383.](#)
675 <https://doi.org/10.1029/2018JD029900>

676 Davies, T. (2014). Lateral boundary conditions for limited area models. *Quarterly Journal of*
677 *the Royal Meteorological Society*, **140**(678), 185-196. <https://doi.org/10.1002/qj.2127>

678 Dentener, F., Kinne, S., Bond, T., Boucher, O., Cofala, J., Generoso, S., et al. (2006). Emissions
679 of primary aerosol and precursor gases in the years 2000 and 1750 prescribed data-sets
680 for AeroCom. *Atmospheric Chemistry and Physics*, **6**, 4321-4344.
681 <https://doi.org/10.5194/acp-6-4321-2006><https://doi.org/10.5194/acp-6-4321-2006>.

682 [Di Luca, A., de Elía, R., and Laprise, R.: Challenges in the Quest for Added Value of Regional](#)
683 [Climate Dynamical Downscaling, Curr. Clim. Change Rep., 1, 10–21,](#)
684 [doi:10.1007/s40641-015-0003-9](https://doi.org/10.1007/s40641-015-0003-9), 2015.

-
- 685 [Diaconescu, E. and Laprise, R.: Can added value be expected in RCM-simulated large scales?,](#)
686 [Clim. Dynam., 41, 1769–1800, doi:10.1007/s00382-012-1649-9,2013.](#)
- 687 Diner, D. J., Beckert, J. C., Reilly, T. H., Bruegge, C. J., Conel, J. E., Kahn, R. A., et al. (1998).
688 Multi-angle Imaging SpectroRadiometer (MISR) - Instrument description and
689 experiment overview. *Ieee Transactions on Geoscience and Remote Sensing*, **36**(4),
690 1072-1087. <https://doi.org/10.1109/36.700992>.
- 691 Diner, D. J., Abdou, W. A., Bruegge, C. J., Conel, J. E., Crean, K. A., Gaitley, B. J., et al.
692 (2001). MISR aerosol optical depth retrievals over southern Africa during the SAFARI-
693 2000 dry season campaign. *Geophysical Research Letters*, **28**(16), 3127-3130.
694 <https://doi.org/10.1029/2001gl013188>
- 695 Ding, Y. H., & Chan, J. C. L. (2005). The East Asian summer monsoon: an overview.
696 *Meteorology and Atmospheric Physics*, **89**(1-4), 117-142.
697 <https://doi.org/10.1007/s00703-005-0125-z>
- 698 Ding, Y. H. (2007). The variability of the Asian summer monsoon. *Journal of the*
699 *Meteorological Society of Japan*, **85b**, 21-54. <https://doi.org/10.2151/jmsj.85B.21>
- 700 Ding, Y. H., Wang, Z. Y., & Sun, Y. (2008). Inter-decadal variation of the summer
701 precipitation in East China and its association with decreasing Asian summer monsoon.
702 Part I: Observed evidences. *International Journal of Climatology*, **28**(9), 1139-1161.
703 <https://doi.org/10.1002/joc.1615>
- 704 Ding, Y. H., Sun, Y., Wang, Z. Y., Zhu, Y. X., & Song, Y. F. (2009). Inter-decadal variation
705 of the summer precipitation in China and its association with decreasing Asian summer
706 monsoon Part II: Possible causes. *International Journal of Climatology*, **29**(13), 1926-
707 1944. <https://doi.org/10.1002/joc.1759>
- 708 Ding, Y., Sun, Y., Liu, Y., Si, D., Wang, Z., Zhu, Y., et al. (2013). Interdecadal and Interannual
709 Variabilities of the Asian Summer Monsoon and Its Projection of Future Change.
710 *Chinese Journal of Atmospheric Sciences*, **37**(2), 253-280.
- 711 Ding, A. J., Fu, C. B., Yang, X. Q., Sun, J. N., Petaja, T., Kerminen, V. M., et al. (2013).
712 Intense atmospheric pollution modifies weather: a case of mixed biomass burning with
713 fossil fuel combustion pollution in eastern China. *Atmospheric Chemistry and Physics*,
714 **13**(20), 10545-10554. <https://doi.org/10.5194/acp-13-10545-2013>
- 715 Dong, B. W., Wilcox, L. J., Highwood, E. J., & Sutton, R. T. (2019). Impacts of recent decadal
716 changes in Asian aerosols on the East Asian summer monsoon: roles of aerosol-
717 radiation and aerosol-cloud interactions. *Climate Dynamics*, **53**(5-6), 3235-3256.
718 <https://doi.org/10.1007/s00382-019-04698-0>

719 Du, Q. Y., Zhao, C., Zhang, M. S., Dong, X., Chen, Y., Liu, Z., et al. (2020). Modeling diurnal
720 variation of surface PM_{2.5} concentrations over East China with WRF-Chem: impacts
721 from boundary-layer mixing and anthropogenic emission. *Atmospheric Chemistry and*
722 *Physics*, **20**(5), 2839-2863. <https://doi.org/10.5194/acp-20-2839-2020>

723 Easter, R. C., Ghan, S. J., Zhang, Y., Saylor, R. D., Chapman, E. G., Laulainen, N. S., et al.
724 (2004). MIRAGE: Model description and evaluation of aerosols and trace gases.
725 *Journal of Geophysical Research-Atmospheres*, **109**(D20).
726 <https://doi.org/10.1029/2004jd004571>

727 European Centre for Medium-Range Weather Forecasts (2019), ERA5 Reanalysis (0.25
728 Degree Latitude-Longitude Grid), <https://doi.org/10.5065/BH6N-5N20>, Research Data
729 Archive at the National Center for Atmospheric Research, Computational and
730 Information Systems Laboratory, Boulder, Colo. (Updated monthly.) Accessed 27 Dec
731 2020.

732 Fan, J. W., Rosenfeld, D., Ding, Y. N., Leung, L. R., & Li, Z. Q. (2012). Potential aerosol
733 indirect effects on atmospheric circulation and radiative forcing through deep
734 convection. *Geophysical Research Letters*, **39**. <https://doi.org/10.1029/2012gl051851>

735 Fan, J. W., Leung, L. R., Rosenfeld, D., Chen, Q., Li, Z. Q., Zhang, J. Q., & Yan, H. R. (201
736 3). Microphysical effects determine macrophysical response for aerosol impacts on de
737 ep convective clouds. *Proceedings of the National Academy of Sciences of the United*
738 *States of America*, **110**(48), E4581-E4590. <https://doi.org/10.1073/pnas.1316830110>

739 Fan, J. W., Rosenfeld, D., Yang, Y., Zhao, C., Leung, L. R., & Li, Z. Q. (2015). Substantial c
740 ontribution of anthropogenic air pollution to catastrophic floods in Southwest China.
741 *Geophysical Research Letters*, **42**(14), 6066-6075. <https://doi.org/10.1002/2015gl064>
742 479

743 Fan, J. W., Wang, Y., Rosenfeld, D., & Liu, X. H. (2016). Review of Aerosol-Cloud Interacti
744 ons: Mechanisms, Significance, and Challenges. *Journal of the Atmospheric Sciences*,
745 **73**(11), 4221-4252. <https://doi.org/10.1175/Jas-D-16-0037.1>

746 Fan, J. W., Rosenfeld, D., Zhang, Y. W., Giangrande, S. E., Li, Z. Q., Machado, L. A. T., et a
747 l. (2018). Substantial convection and precipitation enhancements by ultrafine aerosol
748 particles. *Science*, **359**(6374), 411-418. <https://doi.org/10.1126/science.aan8461>

749 Fast, J. D., Gustafson, W. I., Easter, R. C., Zaveri, R. A., Barnard, J. C., Chapman, E. G., et a
750 l. (2006). Evolution of ozone, particulates, and aerosol direct radiative forcing in the v
751 icinity of Houston using a fully coupled meteorology-chemistry-aerosol model. *Journ*

752 *al of Geophysical Research-Atmospheres*, **111**(D21). [https://doi.org/10.1029/2005jd00](https://doi.org/10.1029/2005jd006721)
753 6721

754 Gao, Y., Zhao, C., Liu, X. H., Zhang, M. G., & Leung, L. R. (2014). WRF-Chem simulations
755 of aerosols and anthropogenic aerosol radiative forcing in East Asia. *Atmospheric Env*
756 *ironment*, **92**, 250-266. <https://doi.org/10.1016/j.atmosenv.2014.04.038>

757 Ginoux, P., Chin, M., Tegen, I., Prospero, J. M., Holben, B., Dubovik, O., & Lin, S. J. (2001).
758 Sources and distributions of dust aerosols simulated with the GOCART model. *Journ*
759 *al of Geophysical Research-Atmospheres*, **106**(D17), 20255-20273. [https://doi.org/10.](https://doi.org/10.1029/2000jd000053)
760 1029/2000jd000053

761 Giorgi, F. (2019). Thirty Years of Regional Climate Modeling: Where Are We and Where Ar
762 e We Going next? *Journal of Geophysical Research-Atmospheres*, **124**(11), 5696-572
763 3. <https://doi.org/10.1029/2018jd030094>

764 Grell, G. A., Peckham, S. E., Schmitz, R., McKeen, S. A., Frost, G., Skamarock, W. C., & Ed
765 er, B. (2005). Fully coupled "online" chemistry within the WRF model. *Atmospheric*
766 *Environment*, **39**(37), 6957-6975. <https://doi.org/10.1016/j.atmosenv.2005.04.027>

767 Guo, L., Highwood, E. J., Shaffrey, L. C., & Turner, A. G. (2013). The effect of regional chan
768 ges in anthropogenic aerosols on rainfall of the East Asian Summer Monsoon. *Atmosp*
769 *heric Chemistry and Physics*, **13**(3), 1521-1534. [https://doi.org/10.5194/acp-13-1521-](https://doi.org/10.5194/acp-13-1521-2013)
770 [2013https://doi.org/10.5194/acp-13-1521-2013.](https://doi.org/10.5194/acp-13-1521-2013)

771 [Hersbach, H, Bell, B, Berrisford, P, et al, 2020: The ERA5 global reanalysis. *Quarterly*
772 *Journal of the Royal Meteorological Society*, **146**, 1999– 2049.](https://doi.org/10.1002/qj.3999)

773 Hu, Z. Y., Zhao, C., Huang, J. P., Leung, L. R., Qian, Y., Yu, H. B., et al. (2016). Trans-Pacif
774 ic transport and evolution of aerosols: evaluation of quasi-global WRF-Chem simulati
775 on with multiple observations. *Geoscientific Model Development*, **9**(5), 1725-1746. [htt](https://doi.org/10.5194/gmd-9-1725-2016)
776 [tps://doi.org/10.5194/gmd-9-1725-2016](https://doi.org/10.5194/gmd-9-1725-2016)

777 Hu, Z. Y., Huang, J. P., Zhao, C., Bi, J. R., Jin, Q. J., Qian, Y., et al. (2019). Modeling the co
778 ntributions of Northern Hemisphere dust sources to dust outflow from East Asia. *Atmo*
779 *spheric Environment*, **202**, 234-243. <https://doi.org/10.1016/j.atmosenv.2019.01.022>

780 Huang, D. L., & Gao, S. B. (2018). Impact of different reanalysis data on WRF dynamical do
781 wnscaling over China. *Atmospheric Research*, **200**, 25-35. [https://doi.org/10.1016/j.at](https://doi.org/10.1016/j.atmosres.2017.09.017)
782 [mosres.2017.09.017](https://doi.org/10.1016/j.atmosres.2017.09.017)

783 Huang, R., & Chen, J. (2010). Characteristics of the Summertime Water Vapor Transports ov
784 er the Eastern Part of China and Those over the Western Part of China and Their Diffe
785 rence. *Chinese Journal of Atmospheric Sciences*, **34**(6), 1035-1046.

786 Huang, X., Ding, A. J., Liu, L. X., Liu, Q., Ding, K., Niu, X. R., et al. (2016). Effects of aerosol-radiation interaction on precipitation during biomass-burning season in East China. *Atmospheric Chemistry and Physics*, **16**(15), 10063-10082. <https://doi.org/10.5194/acp-16-10063-2016>

787
788
789

790 Iacono, M. J., Mlawer, E. J., Clough, S. A., & Morcrette, J. J. (2000). Impact of an improved longwave radiation model, RRTM, on the energy budget and thermodynamic properties of the NCAR community climate model, CCM3. *Journal of Geophysical Research-Atmospheres*, **105**(D11), 14873-14890. <https://doi.org/10.1029/2000jd900091>

791
792
793

794 Iacono, M. J., Delamere, J. S., Mlawer, E. J., Shephard, M. W., Clough, S. A., & Collins, W. D. (2008). Radiative forcing by long-lived greenhouse gases: Calculations with the AER radiative transfer models. *Journal of Geophysical Research-Atmospheres*, **113**(D13). <https://doi.org/10.1029/2008jd009944>

795
796
797

798 IPCC, 2013: *Climate Change 2013: The Physical Science Basis. Contribution of Working Group I to the Fifth Assessment Report of the Intergovernmental Panel on Climate Change* [Stocker, T.F., D. Qin, G.-K. Plattner, M. Tignor, S.K. Allen, J. Boschung, A. Nauels, Y. Xia, V. Bex and P.M. Midgley (eds.)]. Cambridge University Press, Cambridge, United Kingdom and New York, NY, USA, 1535 pp.

799
800
801
802

803 Janssens-Maenhout, G., Crippa, M., Guizzardi, D., Dentener, F., Muntean, M., Pouliot, G., et al. (2015). HTAP_v2.2: a mosaic of regional and global emission grid maps for 2008 and 2010 to study hemispheric transport of air pollution. *Atmospheric Chemistry and Physics*, **15**(19), 11411-11432. <https://doi.org/10.5194/acp-15-11411-2015>

804
805
806

807 Jiang, Y. Q., Liu, X. H., Yang, X. Q., & Wang, M. H. (2013). A numerical study of the effect of different aerosol types on East Asian summer clouds and precipitation. *Atmospheric Environment*, **70**, 51-63. <https://doi.org/10.1016/j.atmosenv.2012.12.039>

808
809

810 Jiang, Z. H., Huo, F., Ma, H. Y., Song, J., & Dai, A. G. (2017). Impact of Chinese Urbanization and Aerosol Emissions on the East Asian Summer Monsoon. *Journal of Climate*, **30**(3), 1019-1039. <https://doi.org/10.1175/Jcli-D-15-0593.1>

811
812

813 Joyce, R. J., Janowiak, J. E., Arkin, P. A., & Xie, P. P. (2004). CMORPH: A method that produces global precipitation estimates from passive microwave and infrared data at high spatial and temporal resolution. *Journal of Hydrometeorology*, **5**(3), 487-503. [https://doi.org/10.1175/1525-7541\(2004\)005<0487:Camtpg>2.0.Co;2](https://doi.org/10.1175/1525-7541(2004)005<0487:Camtpg>2.0.Co;2)

814
815
816

817 Kain, J. S. (2004). The Kain-Fritsch convective parameterization: An update. *Journal of Applied Meteorology*, **43**(1), 170-181. [https://doi.org/10.1175/1520-0450\(2004\)043<0170:Tkcnpau>2.0.Co;2](https://doi.org/10.1175/1520-0450(2004)043<0170:Tkcnpau>2.0.Co;2)

818
819

-
- 820 Kim, M. J., Yeh, S. W., & Park, R. J. (2016). Effects of sulfate aerosol forcing on East Asian
821 summer monsoon for 1985-2010. *Geophysical Research Letters*, **43**(3), 1364-1372.
822 <https://doi.org/10.1002/2015gl067124>
- 823 Kim, M. K., Lau, W. K. M., Kim, K. M., & Lee, W. S. (2007). A GCM study of effects of
824 radiative forcing of sulfate aerosol on large scale circulation and rainfall in East Asia
825 during boreal spring. *Geophysical Research Letters*, **34**(24).
826 <https://doi.org/10.1029/2007gl031683>
- 827 Kok, J. F. (2011). A scaling theory for the size distribution of emitted dust aerosols suggests
828 climate models underestimate the size of the global dust cycle. *Proceedings of the*
829 *National Academy of Sciences of the United States of America*, **108**(3), 1016-1021.
830 <https://doi.org/10.1073/pnas.1014798108>
- 831 Kuniyal, J. C., & Guleria, R. P. (2019). The current state of aerosol-radiation interactions: A
832 mini review. *Journal of Aerosol Science*, **130**, 45-54.
833 <https://doi.org/10.1016/j.jaerosci.2018.12.010>
- 834 Leduc, M., & Laprise, R. (2009). Regional climate model sensitivity to domain size. *Climate*
835 *Dynamics*, **32**(6), 833-854. <https://doi.org/10.1007/s00382-008-0400-z>
- 836 Leduc, M., Laprise, R., Moretti-Poisson, M., & Morin, J. P. (2011). Sensitivity to domain size
837 of mid-latitude summer simulations with a regional climate model. *Climate Dynamics*,
838 **37**(1-2), 343-356. <https://doi.org/10.1007/s00382-011-1008-2>
- 839 Lee, D. K., & Cha, D. H. (2020). Regional climate modeling for Asia. *Geoscience Letters*, **7**(1).
840 <https://doi.org/10.1186/s40562-020-00162-8>
- 841 Li, M., Liu, H., Geng, G. N., Hong, C. P., Liu, F., Song, Y., et al. (2017). Anthropogenic
842 emission inventories in China: a review. *National Science Review*, **4**(6), 834-866.
843 <https://doi.org/10.1093/nsr/nwx150>
- 844 Li, H. M., Dai, A. G., Zhou, T. J., & Lu, J. (2010). Responses of East Asian summer monsoon
845 to historical SST and atmospheric forcing during 1950-2000. *Climate Dynamics*, **34**(4),
846 501-514. <https://doi.org/10.1007/s00382-008-0482-7>
- 847 Li, X. Q., Ting, M. F., Li, C. H., & Henderson, N. (2015). Mechanisms of Asian Summer
848 Monsoon Changes in Response to Anthropogenic Forcing in CMIP5 Models. *Journal*
849 *of Climate*, **28**(10), 4107-4125. <https://doi.org/10.1175/Jcli-D-14-00559.1>
- 850 Li, X. Q., Ting, M. F., & Lee, D. E. (2018). Fast Adjustments of the Asian Summer Monsoon
851 to Anthropogenic Aerosols. *Geophysical Research Letters*, **45**(2), 1001-1010.
852 <https://doi.org/10.1002/2017gl076667>

-
- 853 Li, Z. Q., Lee, K. H., Wang, Y. S., Xin, J. Y., & Hao, W. M. (2010). First observation-based
854 estimates of cloud-free aerosol radiative forcing across China. *Journal of Geophysical*
855 *Research-Atmospheres*, **115**. <https://doi.org/10.1029/2009jd013306>
- 856 Li, Z. Q., Lau, W. K. M., Ramanathan, V., Wu, G., Ding, Y., Manoj, M. G., et al. (2016).
857 Aerosol and monsoon climate interactions over Asia. *Reviews of Geophysics*, **54**(4),
858 866-929. <https://doi.org/10.1002/2015rg000500>
- 859 Li, Z. Q., Wang, Y., Guo, J. P., Zhao, C. F., Cribb, M., Dong, X. Q., et al. (2019). East Asian
860 Study of Tropospheric Aerosols and their Impact on Regional Clouds, Precipitation,
861 and Climate (EAST-AIR(CPC)). *Journal of Geophysical Research-Atmospheres*,
862 **124**(23), 13026-13054. <https://doi.org/10.1029/2019jd030758>
- 863 Liu, H. Y., Jacob, D. J., Bey, I., & Yantosca, R. M. (2001). Constraints from Pb-210 and Be-7
864 on wet deposition and transport in a global three-dimensional chemical tracer model
865 driven by assimilated meteorological fields. *Journal of Geophysical Research-*
866 *Atmospheres*, **106**(D11), 12109-12128. <https://doi.org/10.1029/2000jd900839>
- 867 Liu, J. Z., Li, J., & Li, W. F. (2016). Temporal Patterns in Fine Particulate Matter Time Series
868 in Beijing: A Calendar View. *Scientific Reports*, **6**. <https://doi.org/10.1038/srep32221>
- 869 Luo, Y. X., Zheng, X. B., Zhao, T. L., & Chen, J. (2014). A climatology of aerosol optical
870 depth over China from recent 10 years of MODIS remote sensing data. *International*
871 *Journal of Climatology*, **34**(3), 863-870. <https://doi.org/10.1002/joc.3728>
- 872 Morrison, H., Thompson, G., & Tatarskii, V. (2009). Impact of Cloud Microphysics on the
873 Development of Trailing Stratiform Precipitation in a Simulated Squall Line:
874 Comparison of One- and Two-Moment Schemes. *Monthly Weather Review*, **137**(3),
875 991-1007. <https://doi.org/10.1175/2008mwr2556.1>
- 876 Mlawer, E. J., Taubman, S. J., Brown, P. D., Iacono, M. J., & Clough, S. A. (1997). Radiative
877 transfer for inhomogeneous atmospheres: RRTM, a validated correlated-k model for
878 the longwave. *Journal of Geophysical Research-Atmospheres*, **102**(D14), 16663-16682.
879 <https://doi.org/10.1029/97jd00237>
- 880 Myhre, G., D. Shindell, F.-M. Bréon, W. Collins, J. Fuglestedt, J. Huang, D. Koch, J.-F.
881 Lamarque, D. Lee, B. Mendoza, T. Nakajima, A. Robock, G. Stephens, T. Takemura
882 and H. Zhang, 2013: Anthropogenic and Natural Radiative Forcing. In: Climate Change
883 2013: The Physical Science Basis. Contribution of Working Group I to the Fifth
884 Assessment Report of the Intergovernmental Panel on Climate Change [Stocker, T.F.,
885 D. Qin, G.-K. Plattner, M. Tignor, S.K. Allen, J. Boschung, A. Nauels, Y. Xia, V. Bex

886 and P.M. Midgley (eds.)]. Cambridge University Press, Cambridge, United Kingdom
887 and New York, NY, USA.

888 Nakanishi, M., & Niino, H. (2006). An improved Mellor-Yamada level-3 model: Its numerical
889 stability and application to a regional prediction of advection fog. *Boundary-Layer
890 Meteorology*, **119**(2), 397-407. <https://doi.org/10.1007/s10546-005-9030-8>

891 Nakanishi, M., & Niino, H. (2009). Development of an Improved Turbulence Closure Model
892 for the Atmospheric Boundary Layer. *Journal of the Meteorological Society of Japan*,
893 **87**(5), 895-912. <https://doi.org/10.2151/jmsj.87.895>

894 National Centers for Environmental Prediction/National Weather Service/NOAA/U.S.
895 Department of Commerce (2000), NCEP FNL Operational Model Global Tropospheric
896 Analyses, continuing from July 1999, <https://doi.org/10.5065/D6M043C6>, Research
897 Data Archive at the National Center for Atmospheric Research, Computational and
898 Information Systems Laboratory, Boulder, Colo. (Updated daily.) Accessed 22 Apr
899 2019.

900 Petaja, T., Jarvi, L., Kerminen, V. M., Ding, A. J., Sun, J. N., Nie, W., et al. (2016). Enhanced
901 air pollution via aerosol-boundary layer feedback in China. *Scientific Reports*, **6**.
902 <https://doi.org/10.1038/srep18998>

903 Qi, Y. L., Ge, J. M., & Huang, J. P. (2013). Spatial and temporal distribution of MODIS and
904 MISR aerosol optical depth over northern China and comparison with AERONET.
905 *Chinese Science Bulletin*, **58**(20), 2497-2506. <https://doi.org/10.1007/s11434-013-5678-5>

906

907 Rinke, A., Dethloff, K., & Fortmann, M. (2004). Regional climate effects of Arctic Haze.
908 *Geophysical Research Letters*, **31**(16). <https://doi.org/10.1029/2004gl020318>

909 Rosenfeld, D., Lohmann, U., Raga, G. B., O'Dowd, C. D., Kulmala, M., Fuzzi, S., et al. (2008).
910 Flood or drought: How do aerosols affect precipitation? *Science*, **321**(5894), 1309-1313.
911 <https://doi.org/10.1126/science.1160606>

912 Rosenfeld, D., Andreae, M. O., Asmi, A., Chin, M., de Leeuw, G., Donovan, D. P., et al. (2014).
913 Global observations of aerosol-cloud-precipitation-climate interactions. *Reviews of
914 Geophysics*, **52**(4), 750-808. <https://doi.org/10.1002/2013rg000441>

915 Skamarock, W. C., J. B. Klemp, J. Dudhia, D. O. Gill, D. M. Barker, M. G. Duda, W. Wang,
916 and J. G. Powers (2008), A description of the advanced research WRF version 3, NCAR
917 Tech. Note NCAR/TN-4751STR, 113 pp., Boulder, Colo.

- 918 Schwartz, S. E. (1996). The Whitehouse effect - Shortwave radiative forcing of climate by
919 anthropogenic aerosols: An overview. *Journal of Aerosol Science*, **27**(3), 359-382.
920 [https://doi.org/10.1016/0021-8502\(95\)00533-1](https://doi.org/10.1016/0021-8502(95)00533-1)
- 921 Seth, A., & Giorgi, F. (1998). The effects of domain choice on summer precipitation simulation
922 and sensitivity in a regional climate model. *Journal of Climate*, **11**(10), 2698-2712.
923 [https://doi.org/10.1175/1520-](https://doi.org/10.1175/1520-0442(1998)011<2698:Teodco>2.0.Co;2)
924 [0442\(1998\)011<2698:Teodco>2.0.Co;2](https://doi.org/10.1175/1520-0442(1998)011<2698:Teodco>2.0.Co;2)[https://doi.org/10.1175/1520-](https://doi.org/10.1175/1520-0442(1998)011<2698:Teodco>2.0.Co;2)
925 [0442\(1998\)011<2698:Teodco>2.0.Co;2](https://doi.org/10.1175/1520-0442(1998)011<2698:Teodco>2.0.Co;2)
- 926 [T. Stanelle^{1,*}, B. Vogell¹, H. Vogell¹, D. Baumer^{1,1,*}, and C. Kottmeier: Feedback between](#)
927 [dust particles and atmospheric processes over](#)
928 [West Africa during dust episodes in March 2006 and June 2007, *Atmos. Chem. Phys.*, **10**,](#)
929 [10771–10788, 2010](#)
- 930 Song, F. F., & Zhou, T. J. (2014). The Climatology and Interannual Variability of East Asian
931 Summer Monsoon in CMIP5 Coupled Models: Does Air-Sea Coupling Improve the
932 Simulations? *Journal of Climate*, **27**(23), 8761-8777. [https://doi.org/10.1175/Jcli-D-](https://doi.org/10.1175/Jcli-D-14-00396.1)
933 [14-00396.1](https://doi.org/10.1175/Jcli-D-14-00396.1)
- 934 Song, F. F., Zhou, T. J., & Qian, Y. (2014). Responses of East Asian summer monsoon to
935 natural and anthropogenic forcings in the 17 latest CMIP5 models. *Geophysical*
936 *Research Letters*, **41**(2), 596-603. <https://doi.org/10.1002/2013gl058705>
- 937 Tao, W. K., Chen, J. P., Li, Z. Q., Wang, C., & Zhang, C. D. (2012). Impact of Aerosols on
938 Convective Clouds and Precipitation. *Reviews of Geophysics*, **50**.
939 <https://doi.org/10.1029/2011rg000369>
- 940 Twomey, S. (1977). The influence of pollution on the shortwave albedo of clouds. *Journal of*
941 *the Atmospheric Sciences*, **34**, 1149-1152. [https://doi.org/10.1175/1520-](https://doi.org/10.1175/1520-0469(1977)034<1149:TIOPOT>2.0.CO;2)
942 [0469\(1977\)034<1149:TIOPOT>2.0.CO;2](https://doi.org/10.1175/1520-0469(1977)034<1149:TIOPOT>2.0.CO;2)
- 943 Wang, B., & Yang, H. W. (2008). Hydrological issues in lateral boundary conditions for
944 regional climate modeling: simulation of east asian summer monsoon in 1998. *Climate*
945 *Dynamics*, **31**(4), 477-490. <https://doi.org/10.1007/s00382-008-0385-7>
- 946 Wang, Q. Y., Wang, Z. L., & Zhang, H. (2017). Impact of anthropogenic aerosols from global,
947 East Asian, and non-East Asian sources on East Asian summer monsoon system.
948 *Atmospheric Research*, **183**, 224-236. <https://doi.org/10.1016/j.atmosres.2016.08.023>
- 949 Wang, T., Wang, H. J., Ottera, O. H., Gao, Y. Q., Suo, L. L., Furevik, T., & Yu, L. (2013).
950 Anthropogenic agent implicated as a prime driver of shift in precipitation in eastern

951 China in the late 1970s. *Atmospheric Chemistry and Physics*, **13**(24), 12433-12450.
952 <https://doi.org/10.5194/acp-13-12433-2013>

953 Wang, T. J., Zhuang, B. L., Li, S., Liu, J., Xie, M., Yin, C. Q., et al. (2015). The interactions
954 between anthropogenic aerosols and the East Asian summer monsoon using RegCCMS.
955 *Journal of Geophysical Research-Atmospheres*, **120**(11), 5602-5621.
956 <https://doi.org/10.1002/2014jd022877>

957 Warner, T. T., Peterson, R. A., & Treadon, R. E. (1997). A tutorial on lateral boundary
958 conditions as a basic and potentially serious limitation to regional numerical weather
959 prediction. *Bulletin of the American Meteorological Society*, **78**(11), 2599-2617.
960 [https://doi.org/10.1175/1520-0477\(1997\)078<2599:Atolbc>2.0.Co;2](https://doi.org/10.1175/1520-0477(1997)078<2599:Atolbc>2.0.Co;2)

961 Wiedinmyer, C., Akagi, S. K., Yokelson, R. J., Emmons, L. K., Al-Saadi, J. A., Orlando, J. J.,
962 & Soja, A. J. (2011). The Fire INventory from NCAR (FINN): a high resolution global
963 model to estimate the emissions from open burning. *Geoscientific Model Development*,
964 **4**(3), 625-641. <https://doi.org/10.5194/gmd-4-625-2011>

965 Wu, G. X., Li, Z. Q., Fu, C. B., Zhang, X. Y., Zhang, R. Y., Zhang, R. H., et al. (2016).
966 Advances in studying interactions between aerosols and monsoon in China. *Science*
967 *China-Earth Sciences*, **59**(1), 1-16. <https://doi.org/10.1007/s11430-015-5198-z>

968 Wu, L. T., Su, H., & Jiang, J. H. (2013). Regional simulation of aerosol impacts on precipitation
969 during the East Asian summer monsoon. *Journal of Geophysical Research-*
970 *Atmospheres*, **118**(12), 6454-6467. <https://doi.org/10.1002/jgrd.50527>

971 Xiao, Z. X., & Duan, A. M. (2016). Impacts of Tibetan Plateau Snow Cover on the Interannual
972 Variability of the East Asian Summer Monsoon. *Journal of Climate*, **29**(23), 8495-8514.
973 <https://doi.org/10.1175/Jcli-D-16-0029.1>

974 Xie, X., Wang, H., Liu, X., Li, J., Wang, Z., & Liu, Y. (2016). Distinct effects of anthropogenic
975 aerosols on the East Asian summermonsoon between multidecadal strong and
976 weakmonsoon stages. *Journal of Geophysical Research-Atmospheres*, **121**(12), 7026-
977 7040. <https://doi.org/10.1002/2015jd024228>

978 Xue, Y. K., Janjic, Z., Dudhia, J., Vasic, R., & De Sales, F. (2014). A review on regional
979 dynamical downscaling in intraseasonal to seasonal simulation/prediction and major
980 factors that affect downscaling ability. *Atmospheric Research*, **147**, 68-85.
981 <https://doi.org/10.1016/j.atmosres.2014.05.001>

982 Yan, H. P., Qian, Y., Zhao, C., Wang, H. L., Wang, M. H., Yang, B., et al. (2015). A new
983 approach to modeling aerosol effects on East Asian climate: Parametric uncertainties
984 associated with emissions, cloud microphysics, and their interactions. *Journal of*

985 *Geophysical Research-Atmospheres*, **120**(17), 8905-8924.
986 <https://doi.org/10.1002/2015jd023442>

987 Zaveri, R. A., Easter, R. C., Fast, J. D., & Peters, L. K. (2008). Model for Simulating Aerosol
988 Interactions and Chemistry (MOSAIC). *Journal of Geophysical Research-Atmospheres*,
989 **113**(D13). <https://doi.org/10.1029/2007jd008782>

990 Zaveri, R. A., & Peters, L. K. (1999). A new lumped structure photochemical mechanism for
991 large-scale applications. *Journal of Geophysical Research-Atmospheres*, **104**(D23),
992 30387-30415. <https://doi.org/10.1029/1999jd900876>

993 Zhang, M. X., Zhao, C., Cong, Z. Y., Du, Q. Y., Xu, M. Y., Chen, Y., et al. (2020). Impact of
994 topography on black carbon transport to the southern Tibetan Plateau during the pre-
995 monsoon season and its climatic implication. *Atmospheric Chemistry and Physics*,
996 **20**(10), 5923-5943. <https://doi.org/10.5194/acp-20-5923-2020>

997 Zhang, H., Wang, Z. L., Wang, Z. Z., Liu, Q. X., Gong, S. L., Zhang, X. Y., et al. (2012).
998 Simulation of direct radiative forcing of aerosols and their effects on East Asian climate
999 using an interactive AGCM-aerosol coupled system. *Climate Dynamics*, **38**(7-8), 1675-
1000 1693. <https://doi.org/10.1007/s00382-011-1131-0>

1001 Zhang, R. H. (2015). Changes in East Asian summer monsoon and summer rainfall over eastern
1002 China during recent decades. *Science Bulletin*, **60**(13), 1222-1224.
1003 <https://doi.org/10.1007/s11434-015-0824-x>

1004 Zhang, X. Y., Wang, Y. Q., Niu, T., Zhang, X. C., Gong, S. L., Zhang, Y. M., & Sun, J. Y.
1005 (2012). Atmospheric aerosol compositions in China: spatial/temporal variability,
1006 chemical signature, regional haze distribution and comparisons with global aerosols.
1007 *Atmospheric Chemistry and Physics*, **12**(14), 6273-6273. [https://doi.org/10.5194/acp-](https://doi.org/10.5194/acp-12-6273-2012)
1008 [12-6273-2012](https://doi.org/10.5194/acp-12-6273-2012)

1009 Zhao, B., Liou, K. N., Gu, Y., Li, Q. B., Jiang, J. H., Su, H., et al. (2017). Enhanced PM2.5
1010 pollution in China due to aerosol-cloud interactions. *Scientific Reports*, **7**.
1011 <https://doi.org/10.1038/s41598-017-04096-8>

1012 Zhao, C., Liu, X., Leung, L. R., Johnson, B., McFarlane, S. A., Gustafson, W. I., et al. (2010).
1013 The spatial distribution of mineral dust and its shortwave radiative forcing over North
1014 Africa: modeling sensitivities to dust emissions and aerosol size treatments.
1015 *Atmospheric Chemistry and Physics*, **10**(18), 8821-8838. [https://doi.org/10.5194/acp-](https://doi.org/10.5194/acp-10-8821-2010)
1016 [10-8821-2010](https://doi.org/10.5194/acp-10-8821-2010)

-
- 1017 Zhao, C., Liu, X., Leung, L. R., & Hagos, S. (2011). Radiative impact of mineral dust on
1018 monsoon precipitation variability over West Africa. *Atmospheric Chemistry and*
1019 *Physics*, **11**(5), 1879-1893. <https://doi.org/10.5194/acp-11-1879-2011>
- 1020 Zhao, C., Liu, X., & Leung, L. R. (2012). Impact of the Desert dust on the summer monsoon
1021 system over Southwestern North America. *Atmospheric Chemistry and Physics*, **12**(8),
1022 3717-3731. <https://doi.org/10.5194/acp-12-3717-2012>
- 1023 Zhao, C., Chen, S., Leung, L. R., Qian, Y., Kok, J. F., Zaveri, R. A., & Huang, J. (2013a).
1024 Uncertainty in modeling dust mass balance and radiative forcing from size
1025 parameterization. *Atmospheric Chemistry and Physics*, **13**(21), 10733-10753.
1026 <https://doi.org/10.5194/acp-13-10733-2013>
- 1027 Zhao, C., Leung, L. R., Easter, R., Hand, J., & Avise, J. (2013b). Characterization of speciated
1028 aerosol direct radiative forcing over California. *Journal of Geophysical Research-*
1029 *Atmospheres*, **118**(5), 2372-2388. <https://doi.org/10.1029/2012jd018364>
- 1030 Zhao, C., Hu, Z., Qian, Y., Leung, L. R., Huang, J., Huang, M., et al. (2014). Simulating black
1031 carbon and dust and their radiative forcing in seasonal snow: a case study over North
1032 China with field campaign measurements. *Atmospheric Chemistry and Physics*, **14**(20),
1033 11475-11491. <https://doi.org/10.5194/acp-14-11475-2014>
- 1034 Zhao, C., Huang, M. Y., Fast, J. D., Berg, L. K., Qian, Y., Guenther, A., et al. (2016).
1035 Sensitivity of biogenic volatile organic compounds to land surface parameterizations
1036 and vegetation distributions in California. *Geoscientific Model Development*, **9**(5),
1037 1959-1976. <https://doi.org/10.5194/gmd-9-1959-2016>
- 1038 Zheng, B., Tong, D., Li, M., Liu, F., Hong, C. P., Geng, G. N., et al. (2018). Trends in China's
1039 anthropogenic emissions since 2010 as the consequence of clean air actions.
1040 *Atmospheric Chemistry and Physics*, **18**(19), 14095-14111.
1041 <https://doi.org/10.5194/acp-18-14095-2018>
- 1042 Zhou, T. J., Gong, D. Y., Li, J., & Li, B. (2009). Detecting and understanding the multi-decadal
1043 variability of the East Asian Summer Monsoon - Recent progress and state of affairs.
1044 *Meteorologische Zeitschrift*, **18**(4), 455-467. [https://doi.org/10.1127/0941-](https://doi.org/10.1127/0941-2948/2009/0396)
1045 [2948/2009/0396](https://doi.org/10.1127/0941-2948/2009/0396)
- 1046 Zhu, Y. L., Wang, H. J., Zhou, W., & Ma, J. H. (2011). Recent changes in the summer
1047 precipitation pattern in East China and the background circulation. *Climate Dynamics*,
1048 **36**(7-8), 1463-1473. <https://doi.org/10.1007/s00382-010-0852-9>
- 1049 Zhuang, B. L., Li, S., Wang, T. J., Liu, J., Chen, H. M., Chen, P. L., et al. (2018). Interaction
1050 between the Black Carbon Aerosol Warming Effect and East Asian Monsoon Using

1051 RegCM4. *Journal of Climate*, **31**(22), 9367-9388. [https://doi.org/10.1175/Jcli-D-17-](https://doi.org/10.1175/Jcli-D-17-0767.1)
1052 [0767.1](https://doi.org/10.1175/Jcli-D-17-0767.1).

1053 [Zhang, D., A. Zakey, X. Gao, F. Giorgi, and F. Solomon: Simulation of dust aerosol and its](#)
1054 [regional feedbacks over East Asia using a regional climate model, *Atmos. Chem. Phys.*,](#)
1055 [9, 1095–1110, 2009.](#)

1056

1057

1058

1059
 1060
 1061
 1062
 1063

Table 1. Experiment Description.

| Experiment ID | Experiment Description |
|---------------|--|
| CTRL-L | Control experiment with large simulation domain. |
| CLEAN-L | Same <u>Similar</u> as CTRL-L, but the anthropogenic aerosol emissions are 0.1 times of CTRL-L. |
| CTRL-S | Control experiment with small simulation domain. |
| CLEAN-S | Same <u>Similar</u> as CTRL-S, but the anthropogenic aerosol emissions are 0.1 times of CTRL-S. |
| <u>NoRA-S</u> | <u>Similar as CTRL-S, but with the aerosol-radiation interaction turned off.</u> |

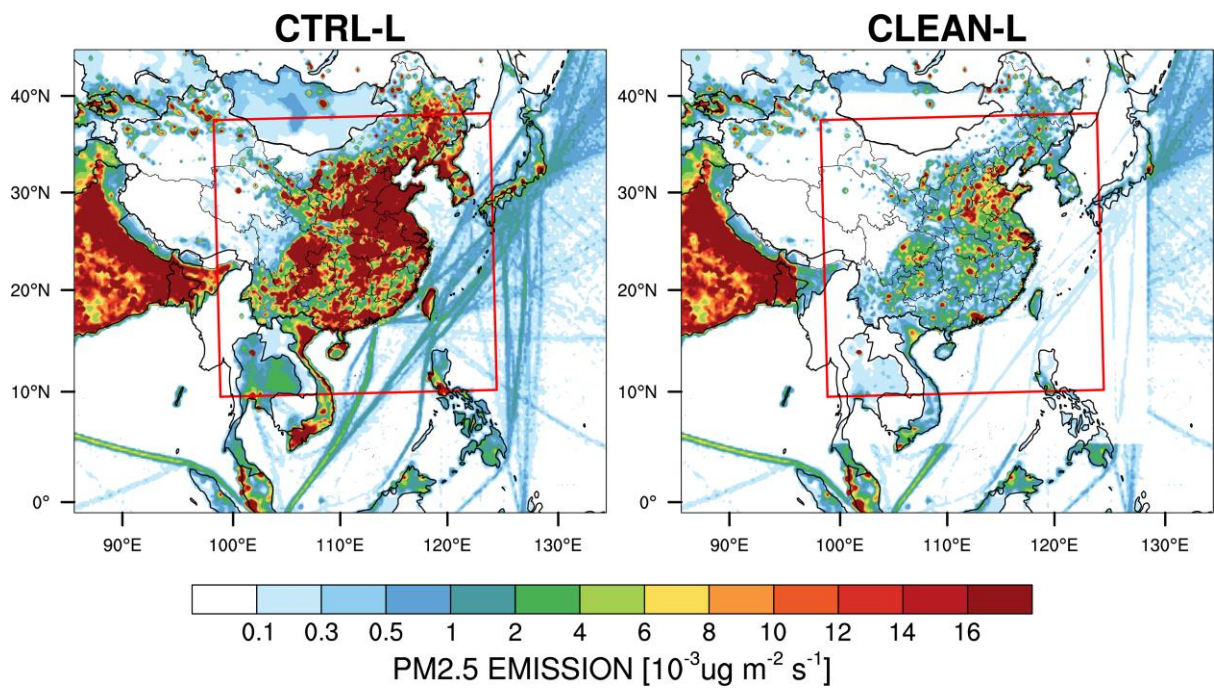
1064
 1065
 1066
 1067
 1068

1069 **Table 2.** Summary of model configurations.

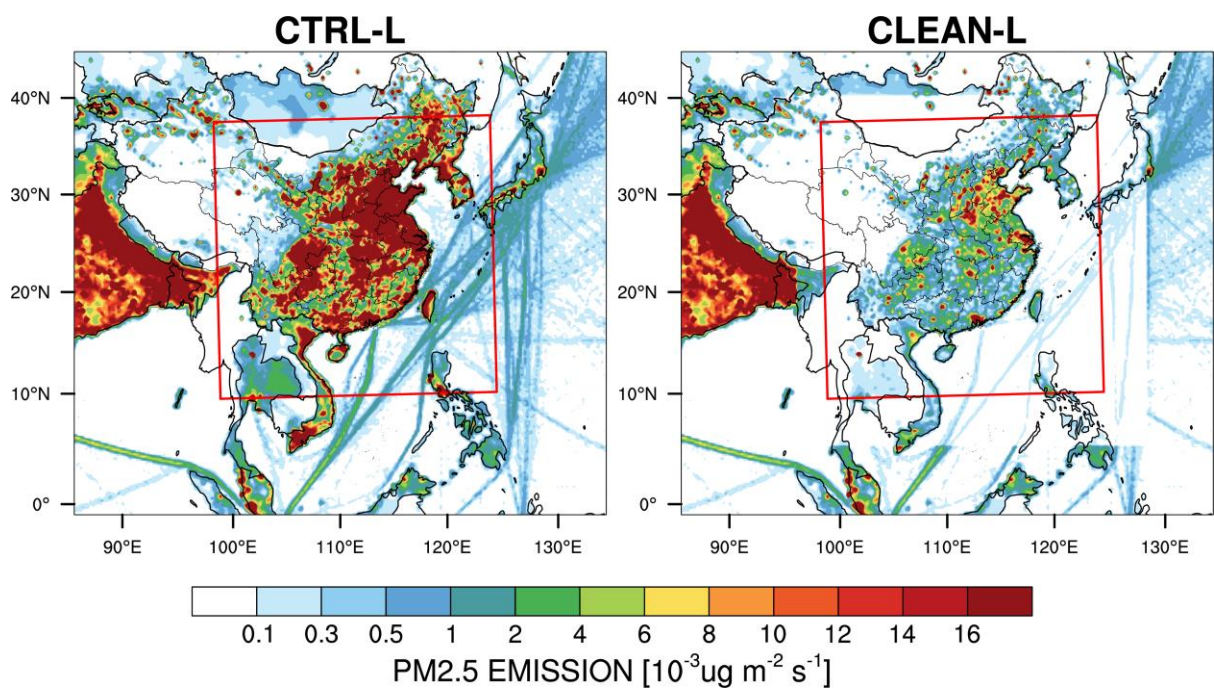
| Description | Selection_(L, S) |
|--------------------------|---------------------------------|
| Horizontal grid spacing | 30km |
| Grid dimensions | 201x231, 121x121 |
| Vertical layers | 41 |
| Topography | USGS_30s |
| Model top press | 100hPa |
| Aerosol scheme | MOSAIC 4 bin |
| Gas-phase chemistry | CBM-Z |
| Long wave Radiation | RRTMG |
| Short wave Radiation | RRTMG |
| Cloud Microphysics | Morrison 2-moment |
| Cumulus Cloud | Kain-Fritsch |
| Planetary boundary layer | MYNN 3rd |
| Land surface | unified Noah land-surface model |
| Meteorological Forcing | FNL, 1°x1° ,6 hourly |

1070
 1071
 1072
 1073

1074
1075
1076
1077
1078
1079
1080

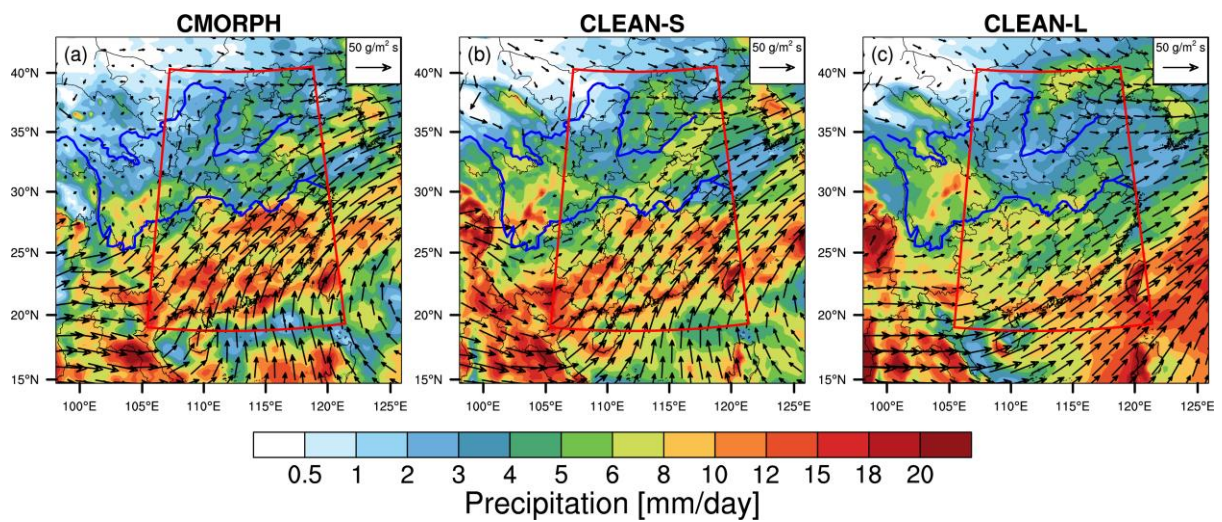


1081

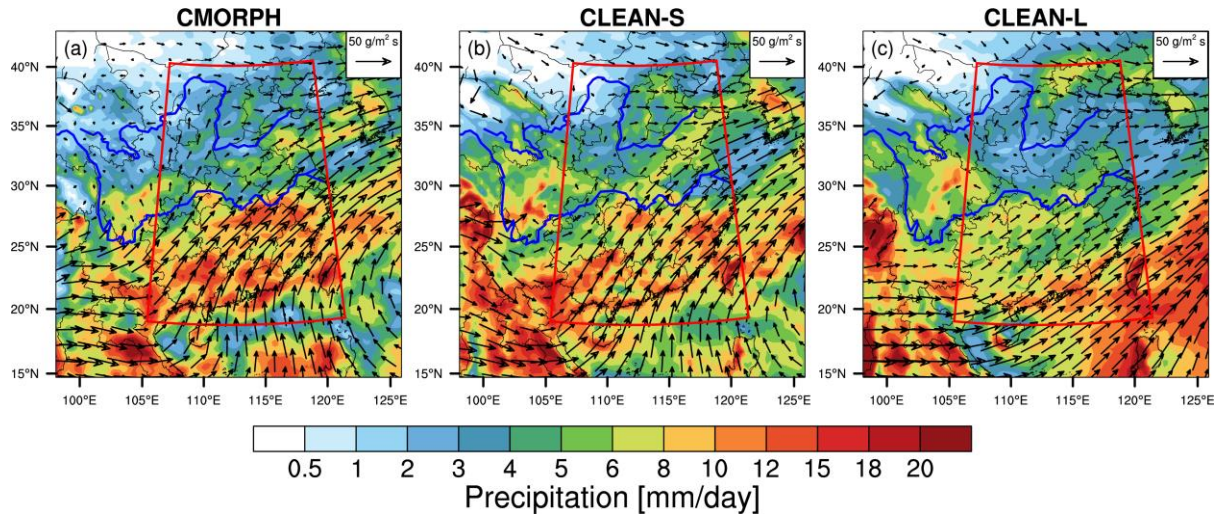


1082

1083 **Figure 1.** Spatial distributions of anthropogenic emissions of primary PM_{2.5} averaged for June
1084 and July for the simulation domains. The red box in the large simulation domain represents the
1085 small domain.
1086
1087
1088
1089
1090
1091
1092
1093
1094
1095
1096
1097
1098
1099
1100
1101
1102
1103
1104
1105
1106
1107



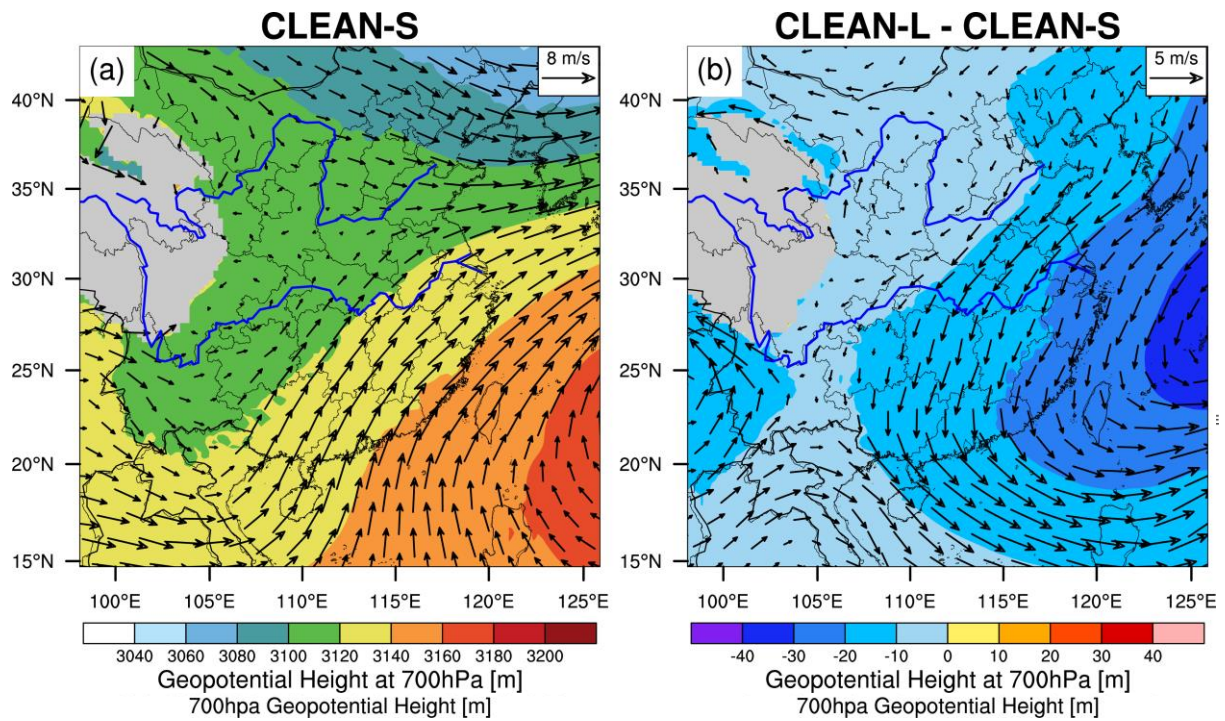
1108
1109



1110
 1111
 1112
 1113
 1114
 1115
 1116
 1117
 1118
 1119
 1120
 1121
 1122
 1123
 1124
 1125
 1126
 1127
 1128
 1129
 1130
 1131
 1132
 1133
 1134
 1135
 1136
 1137
 1138
 1139
 1140

Figure 2. Mean precipitation rate (mm/day) and 700hPa moisture transport ($\text{g/m}^2 \text{s}$) over the small domain for the two months of June and July 2017 from (a) CMORPH and ERA5 reanalysis, (b) CLEAN-S simulation, and (c) CLEAN-L simulation. The red box (20°N - 42°N , 105°E - 122°E) represents the focus area of analysis in follow. (a) Precipitation data comes from CMORPH, and the 700hPa moisture transport field data is obtained by processing ERA5 reanalysis.

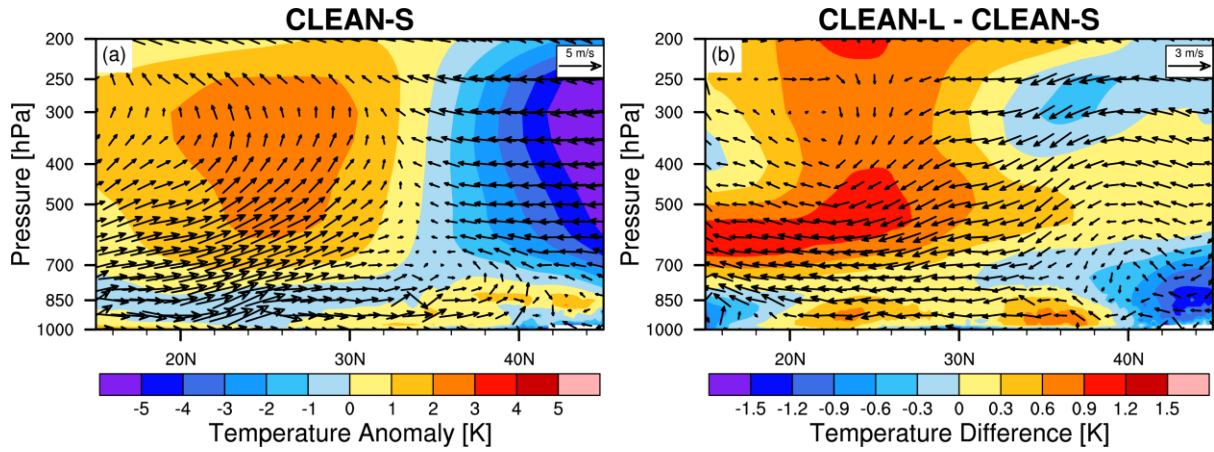
1141
1142



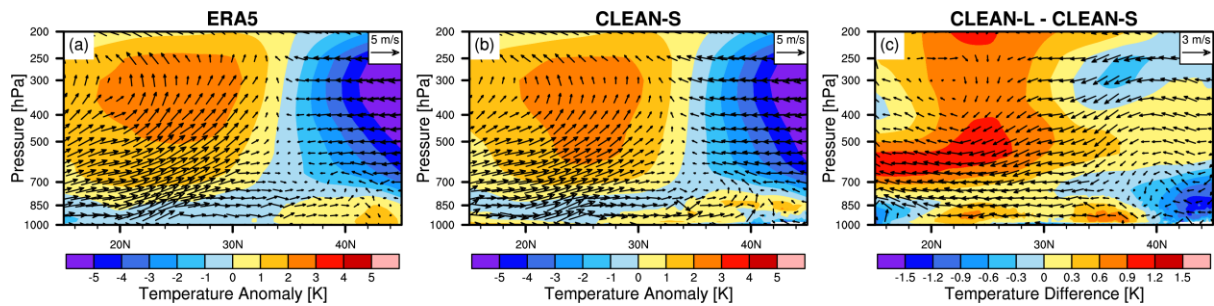
1143
1144
1145
1146
1147
1148
1149
1150
1151
1152
1153
1154
1155
1156
1157
1158
1159
1160
1161
1162
1163
1164
1165
1166
1167

Figure 3. Spatial ~~distribution~~distributions of mean geopotential height and wind fields at 700 hPa Geopotential Height and winds of June and July 2017 from (a) ERA5, (b) CLEAN-S, and ~~the (b)(c)~~ difference between CLEAN-L and CLEAN-S.

1168
1169
1170
1171



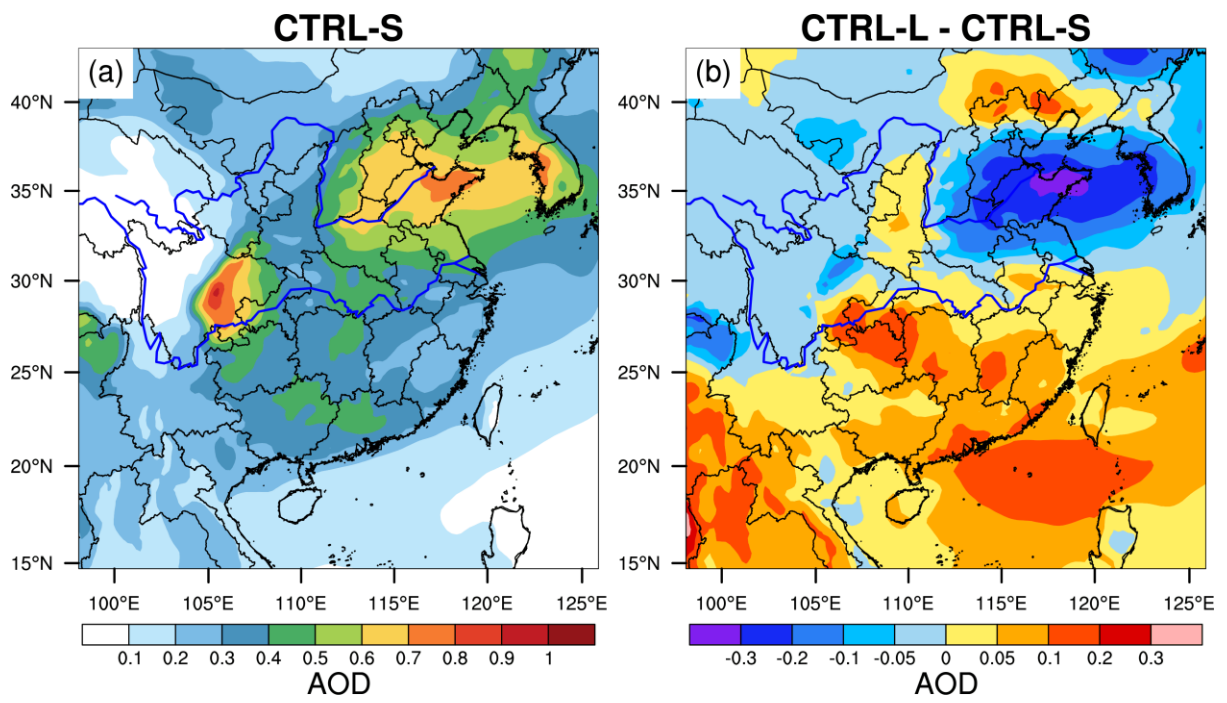
1172
1173
1174
1175
1176
1177



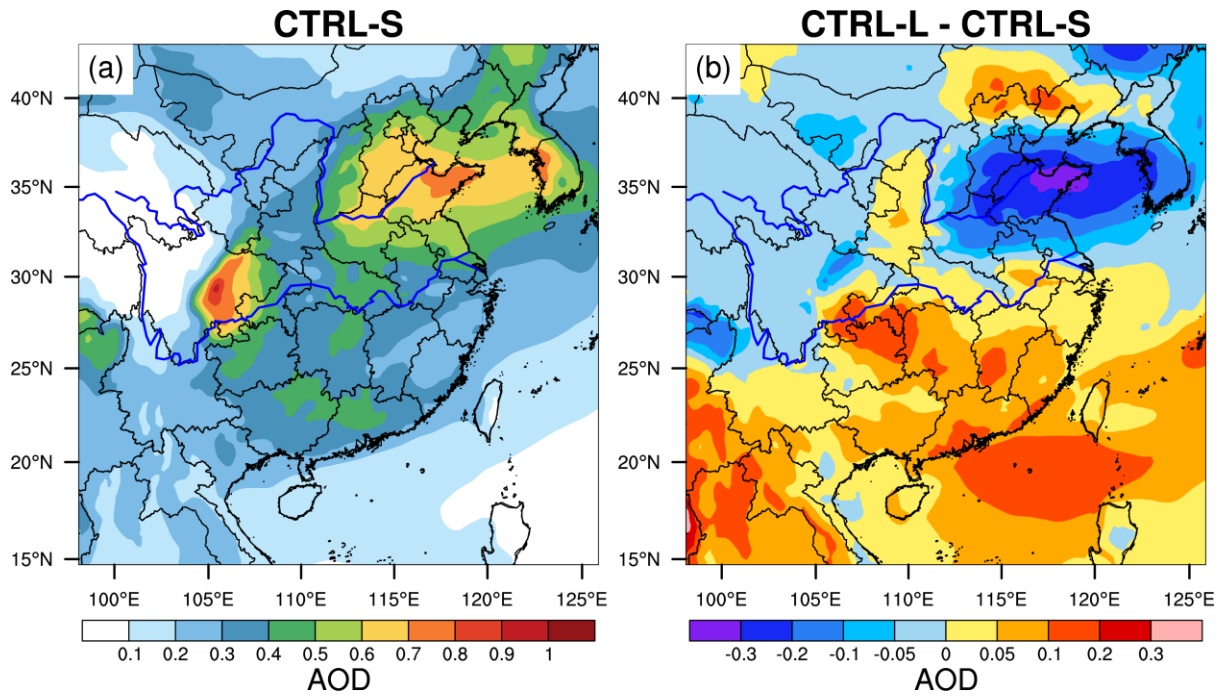
1178 **Figure 4.** (a, b) The cross-section of meridional temperature anomalies and wind averaged for
1179 105°E and 122°E from (a) the ERA5 reanalysis and the CLEAN-S simulation during June to
1180 July, and (bc) the difference of temperature (not meridional temperature anomalies) between
1181 CLEAN-L and CLEAN-S. The meridional temperature anomalies are calculated by subtracting
1182 the mean temperature in this latitude range at each pressure level.

1183
1184
1185
1186
1187
1188
1189
1190
1191
1192

1193
1194
1195
1196
1197
1198
1199
1200
1201
1202
1203
1204
1205
1206
1207
1208
1209

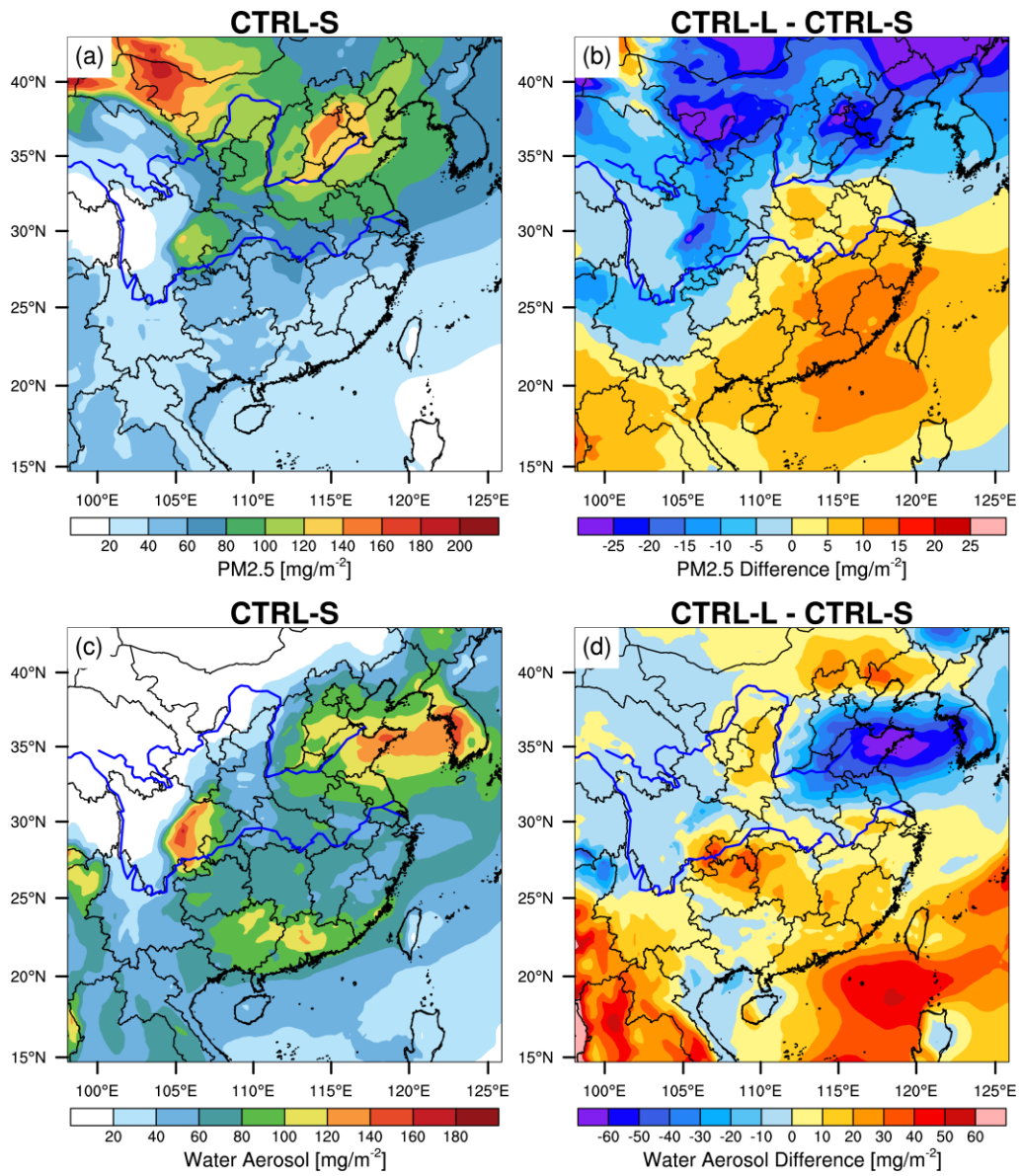


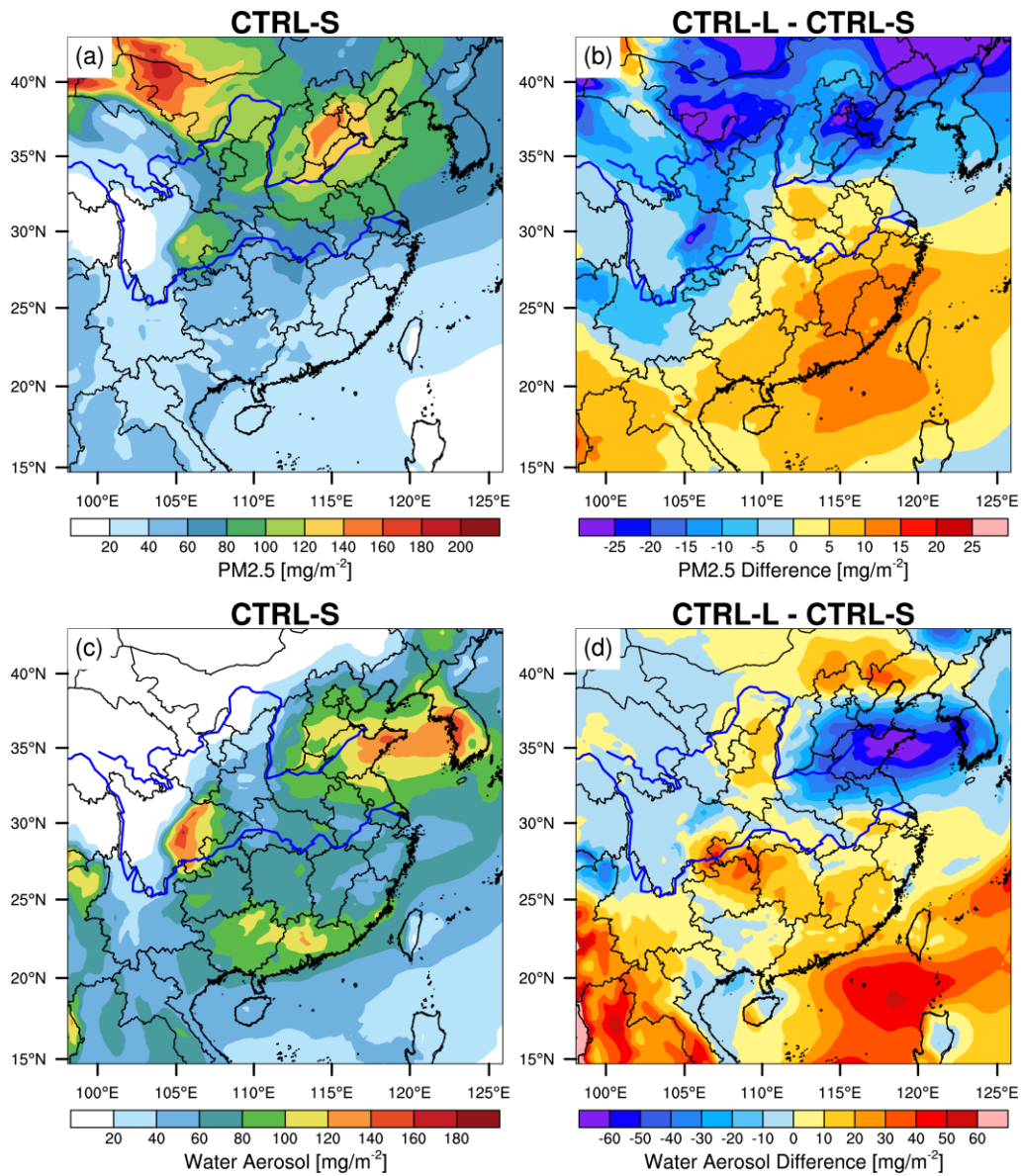
1210
1211



1212
 1213
 1214
 1215
 1216
 1217
 1218
 1219
 1220
 1221
 1222
 1223
 1224
 1225
 1226
 1227
 1228
 1229
 1230
 1231
 1232

Figure 5. The spatial ~~distribution~~distributions of AOD for June and July of 2017 from the CTRL-S simulation, and the difference between CTRL-L and CTRL-S.





1237

1238

Figure 6. The spatial distributions of column integrated total (a) PM_{2.5} concentration and (c)

water content in aerosol averaged for June and July of 2017 from the CTRL-S simulation, and

1240

(b) and (d) the difference between CTRL-L and CTRL-S.

1241

1242

1243

1244

1245

1246

1247

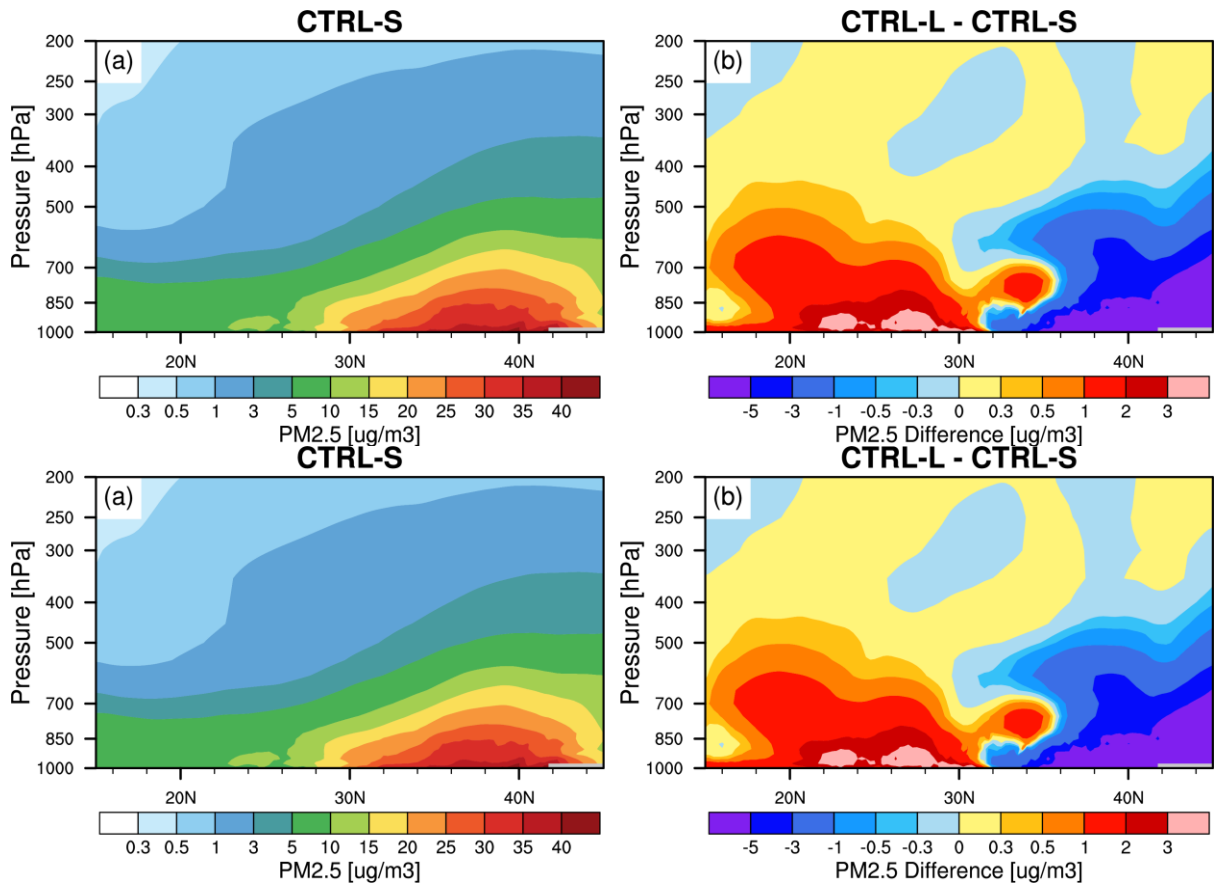
1248

1249

1250

1251

1252
1253
1254
1255
1256
1257



1258

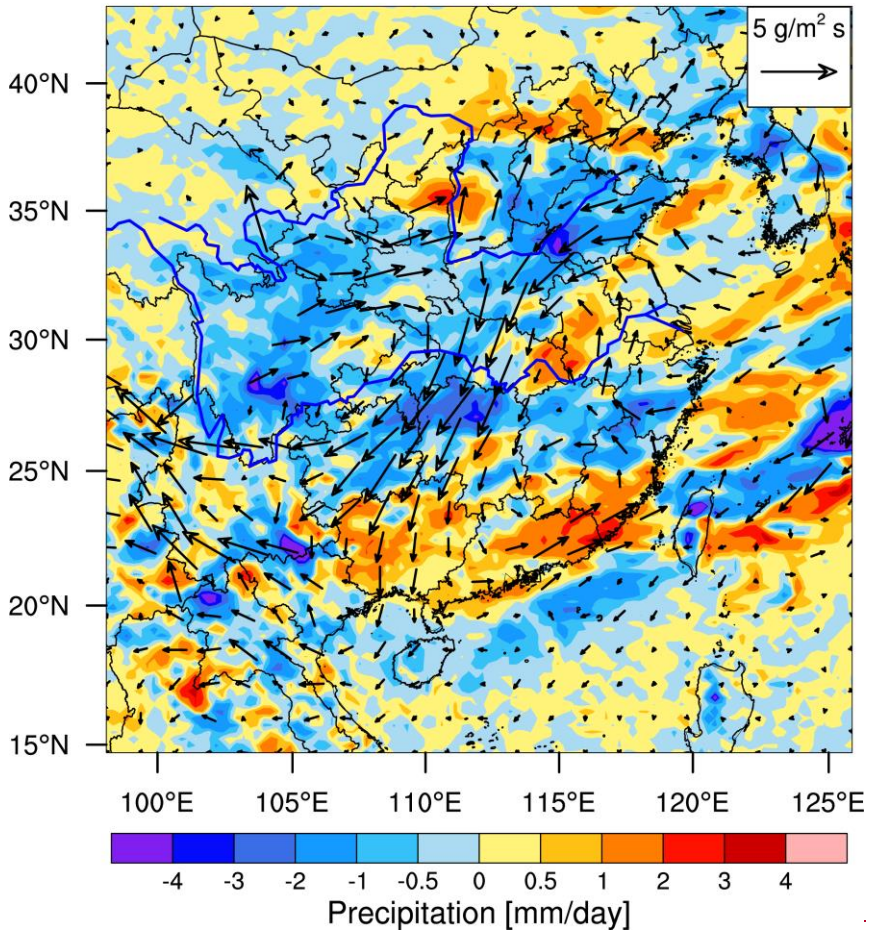
1259

Figure 7. The latitude-height cross-section of (a) total $PM_{2.5}$ averaged between $105^{\circ}E$ and $122^{\circ}E$ for June and July of 2017 from the CTRL-S experiment, and (b) the difference between CTRL-L and CTRL-S.

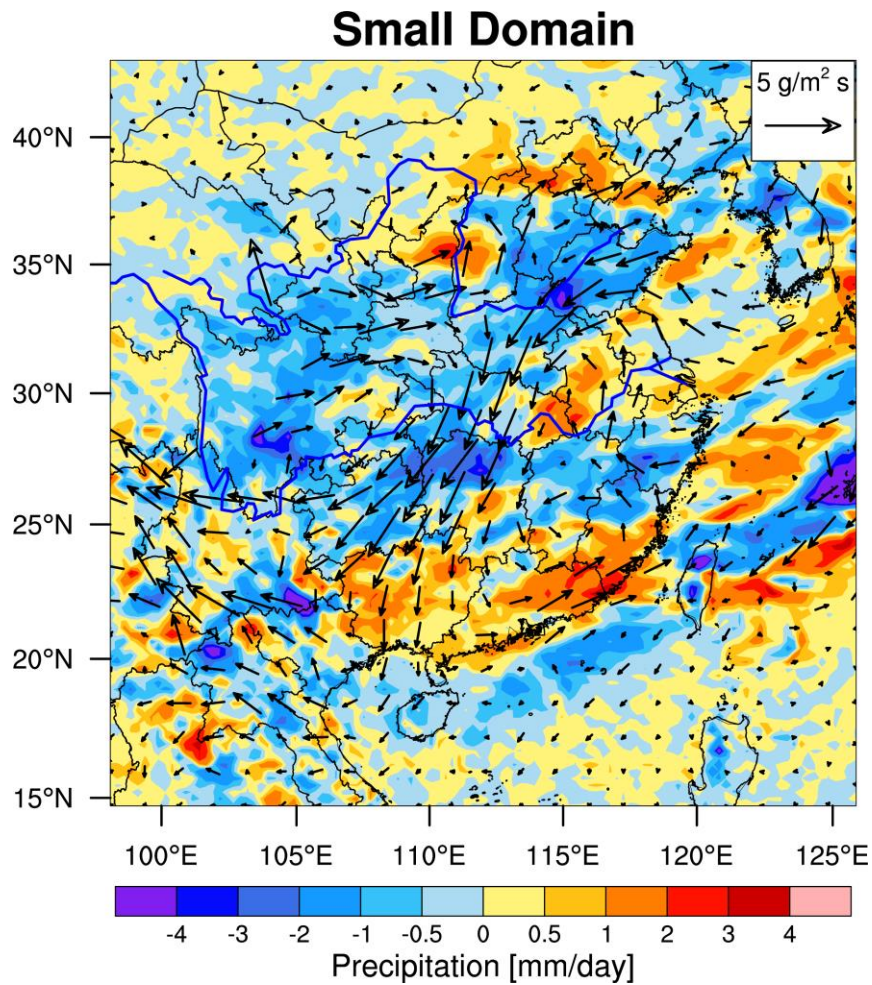
1263
1264
1265
1266
1267
1268
1269
1270
1271
1272
1273
1274
1275
1276

1277
1278
1279
1280
1281
1282
1283
1284
1285
1286
1287
1288
1289
1290
1291

Small Domain



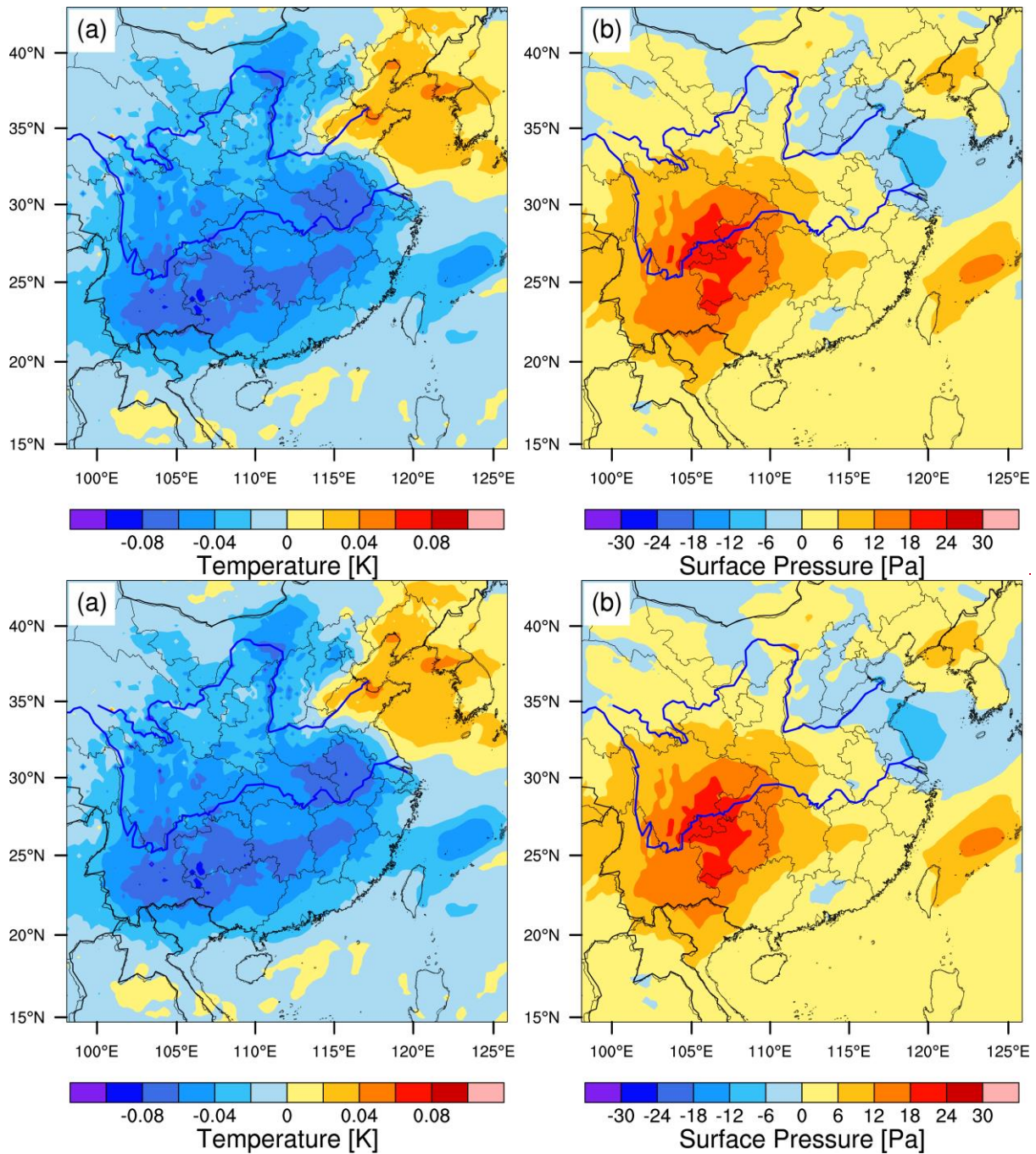
1292



1293
 1294
 1295
 1296
 1297
 1298
 1299
 1300
 1301
 1302
 1303
 1304
 1305
 1306
 1307
 1308
 1309
 1310
 1311
 1312
 1313
 1314
 1315
 1316

Figure 8. The spatial distributions of aerosol-induced difference (CTRL-CLEAN) of precipitation and moisture transport at 700 hPa averaged for June and July of 2017 from the small domain simulations.

1317
1318



1319

1320

Figure 9. The spatial distributions of aerosol-induced difference (CTRL-CLEAN) of (a) atmosphere temperature below 500 hPa and (b) surface pressure averaged for June and July of 2017 from the small domain simulations. ~~We interpolate the atmosphere~~ Atmospheric temperature to the isobaric surface is weight-averaged by the layer thickness below 500 hPa and get the atmosphere temperature below 500 hPa by weighted average according to the layer height.

1327

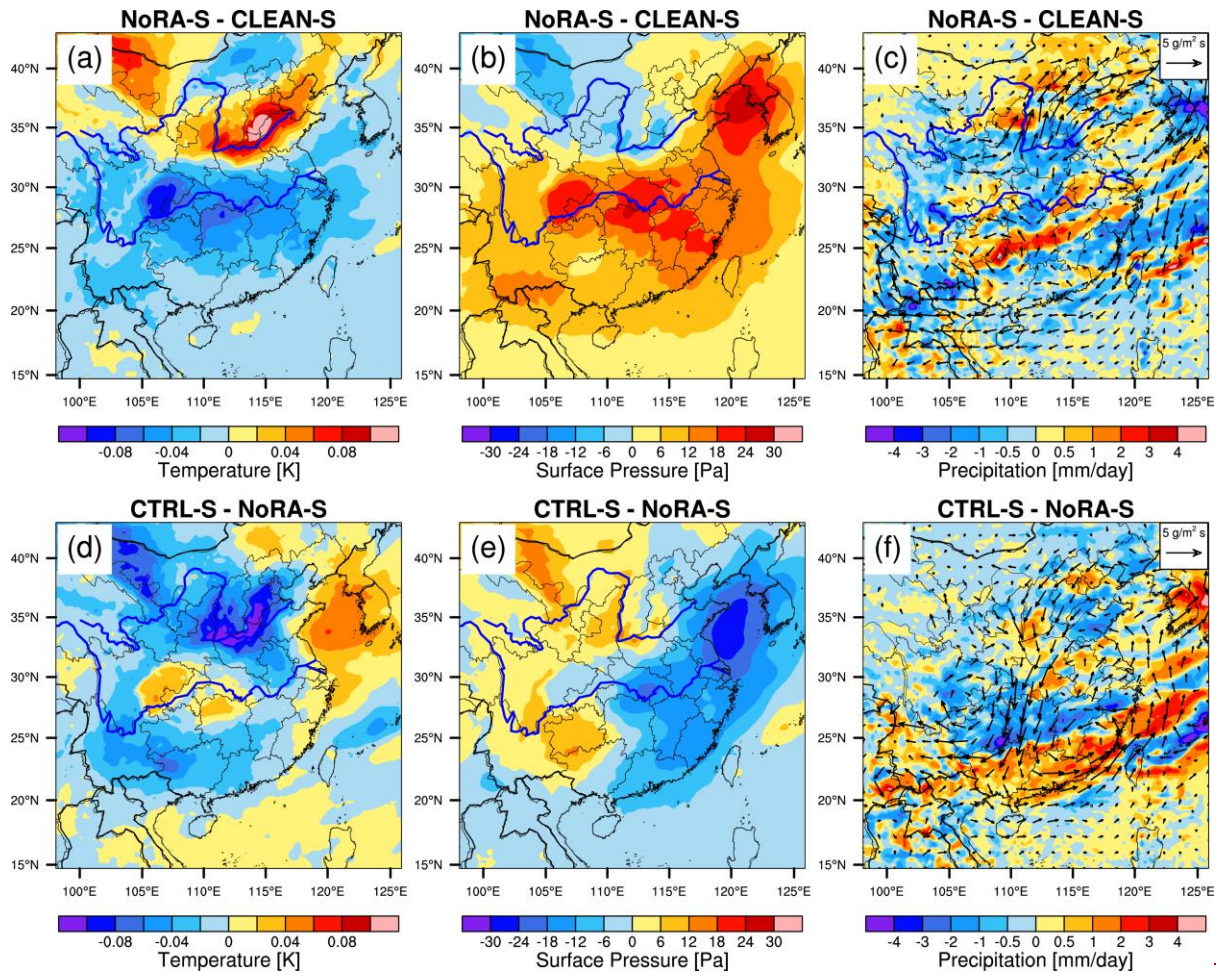
1328

1329

1330

1331

1332
1333
1334
1335
1336
1337
1338
1339
1340
1341
1342
1343
1344
1345
1346
1347
1348



1349
1350

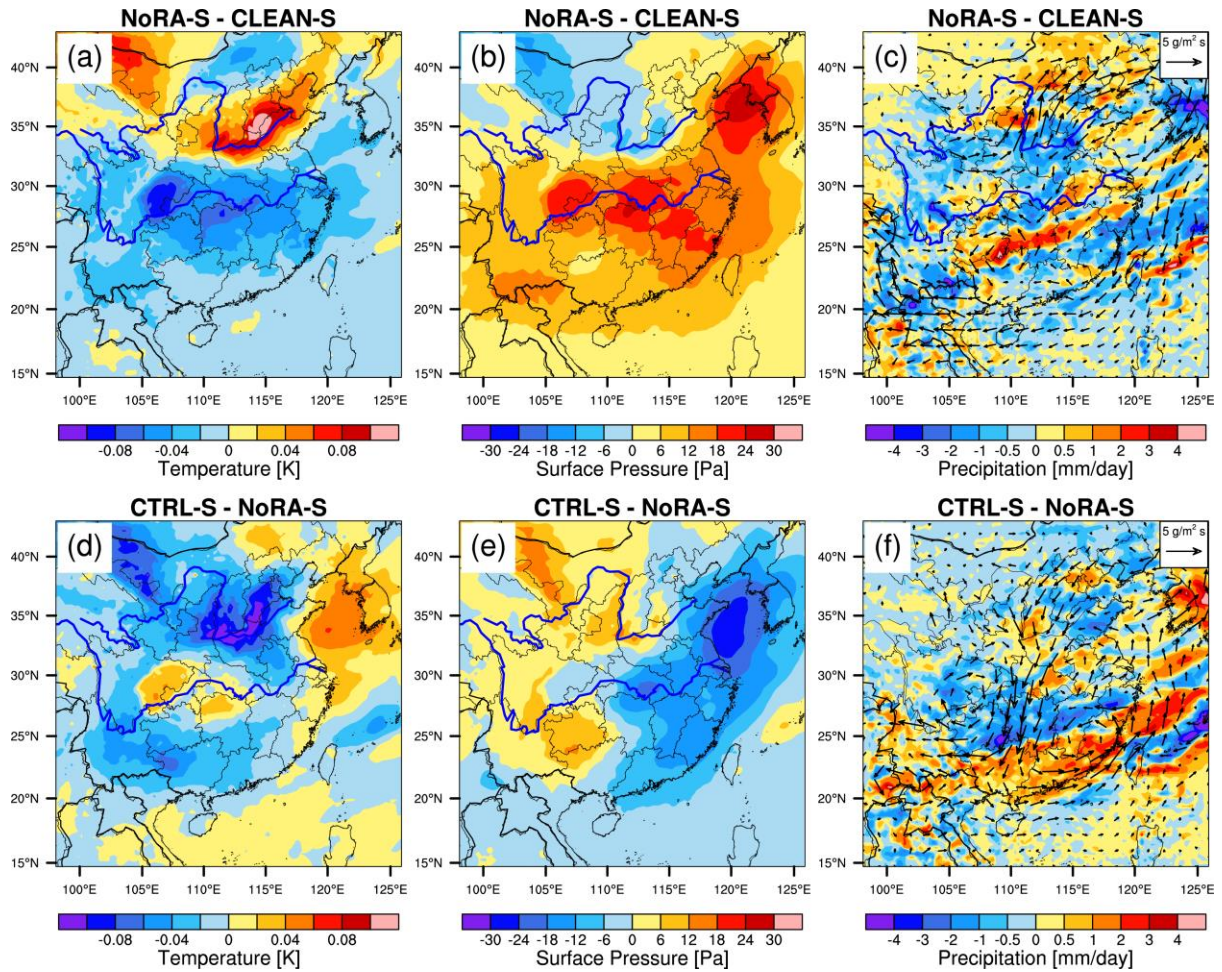
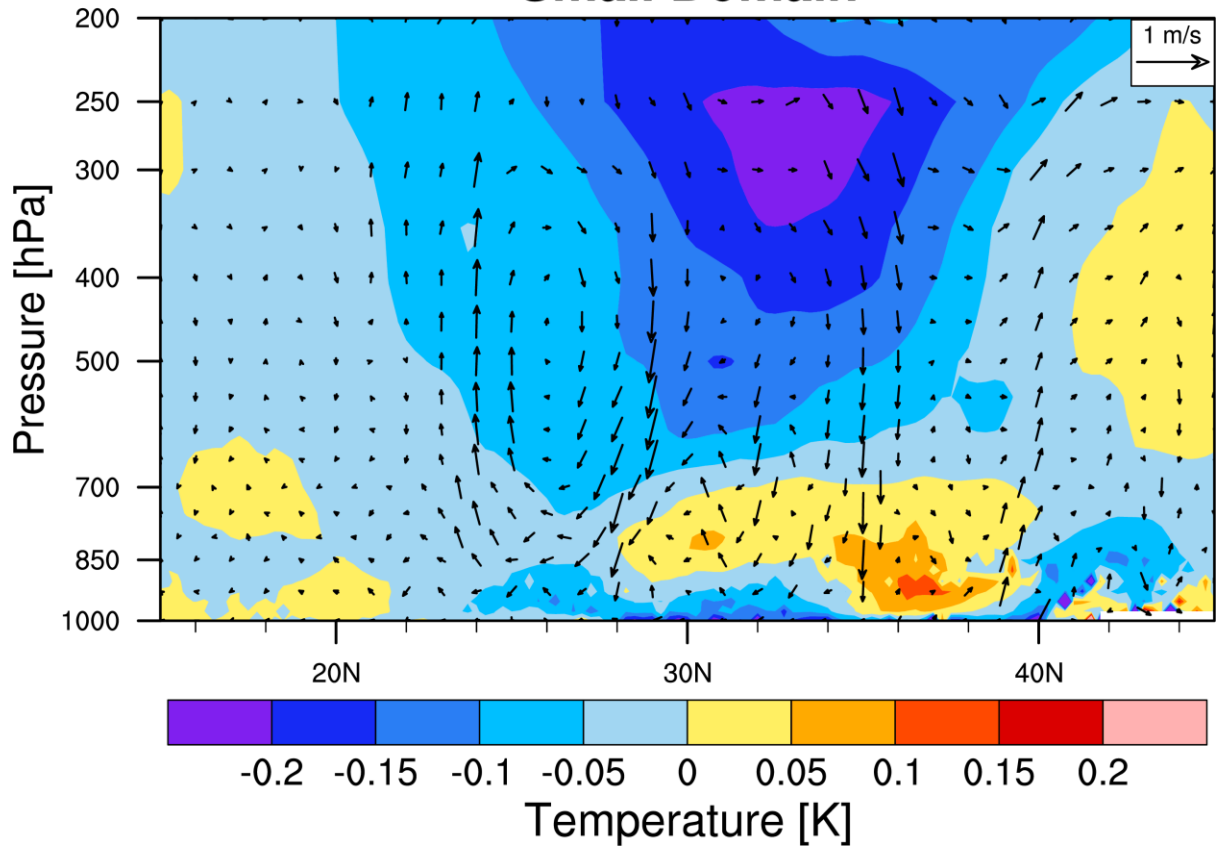


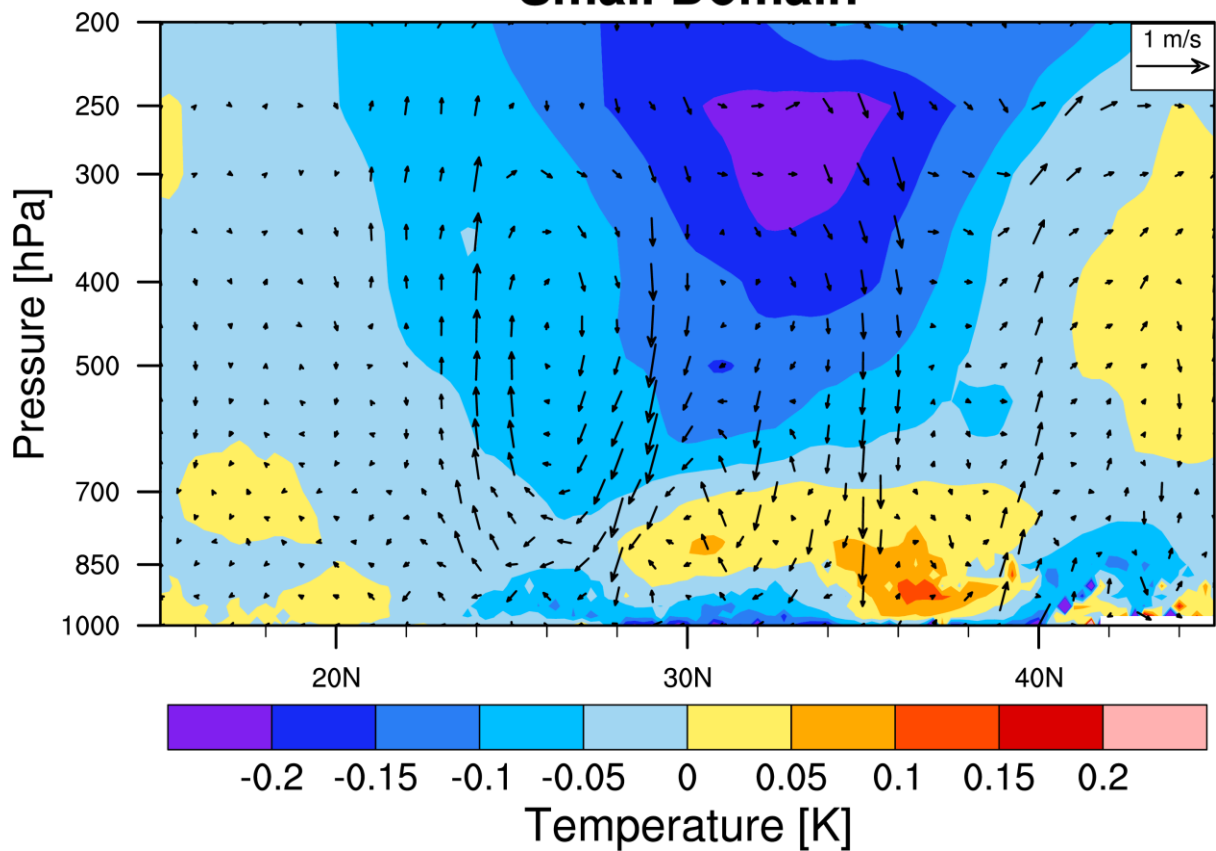
Figure 10. The spatial distributions of Aerosol-Cloud interactions induced difference of (a) atmosphere temperature below 500 hPa, (b) surface pressure and (c) precipitation and moisture transport at 700 hPa averaged for June and July of 2017 from the small domain simulations. And the spatial distributions of Aerosol-Radiation interactions induced difference of (d) atmosphere temperature below 500 hPa, (e) surface pressure and (f) precipitation and moisture transport at 700 hPa averaged for June and July of 2017 from the small domain simulations.

1351
 1352
 1353
 1354
 1355
 1356
 1357
 1358
 1359
 1360
 1361
 1362
 1363
 1364
 1365
 1366
 1367
 1368
 1369
 1370
 1371
 1372
 1373
 1374
 1375

Small Domain



Small Domain

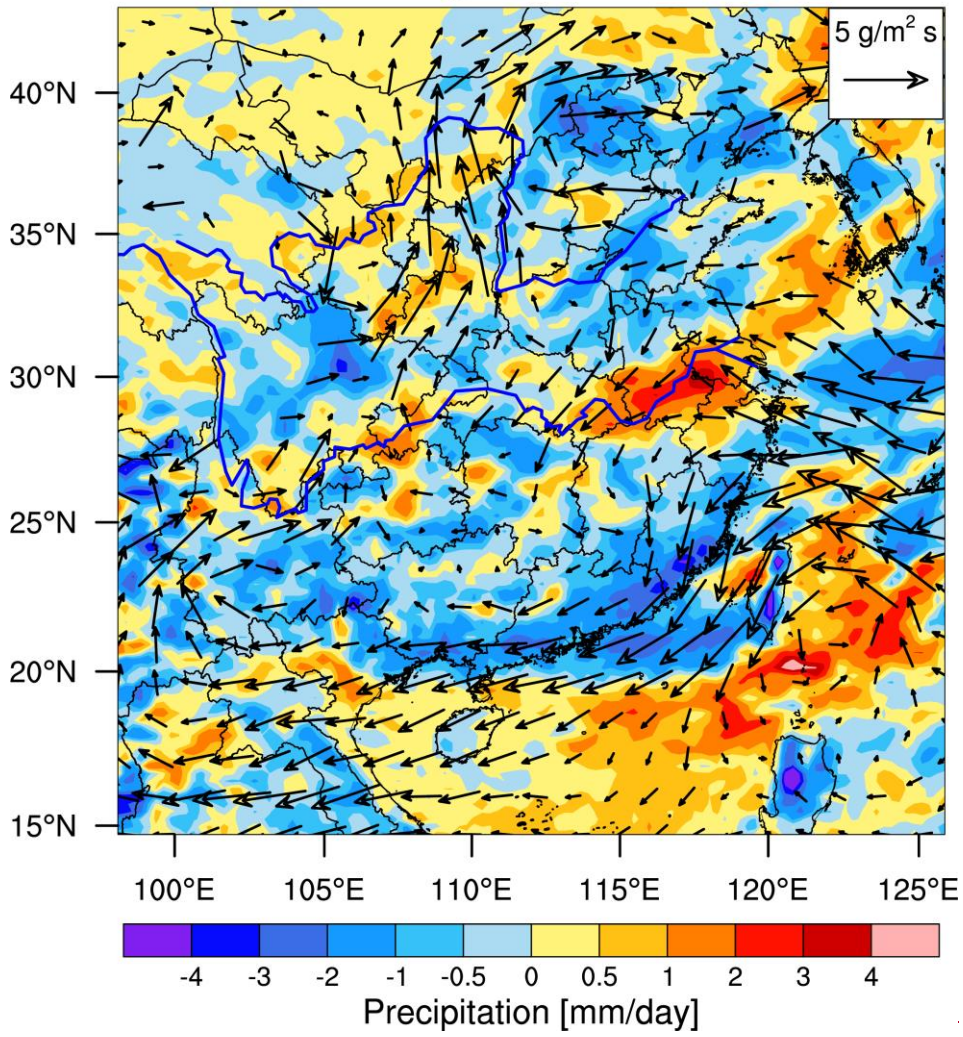


1376
1377
1378

1379

1380 **Figure 11.** The latitude-pressure cross-section of aerosol-induced difference (CTRL-CLEAN)
1381 of temperature and wind averaged between 105°E and 122°E for June and July of 2017 from
1382 the small domain simulation.
1383
1384
1385
1386
1387
1388
1389
1390
1391
1392
1393
1394
1395
1396
1397
1398
1399
1400
1401
1402
1403
1404

Large Domain



1405

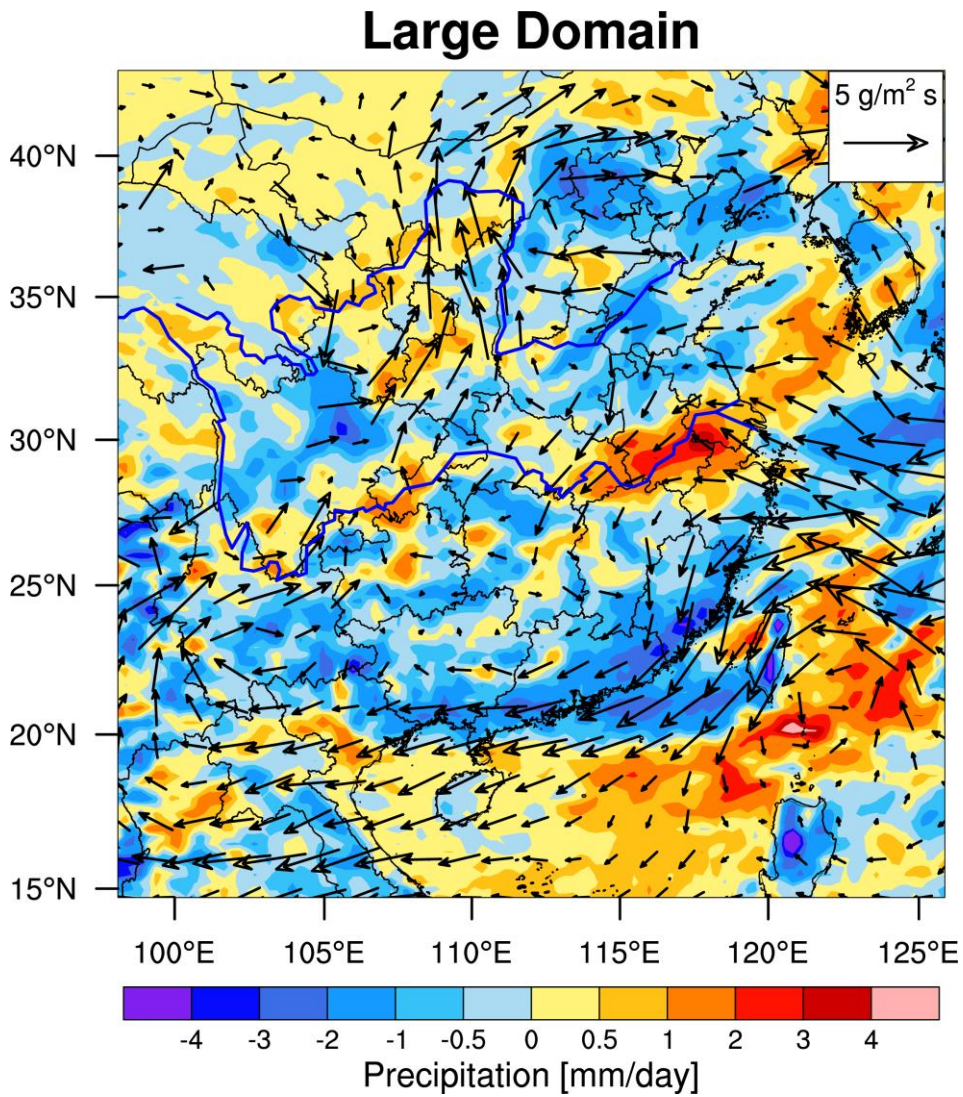
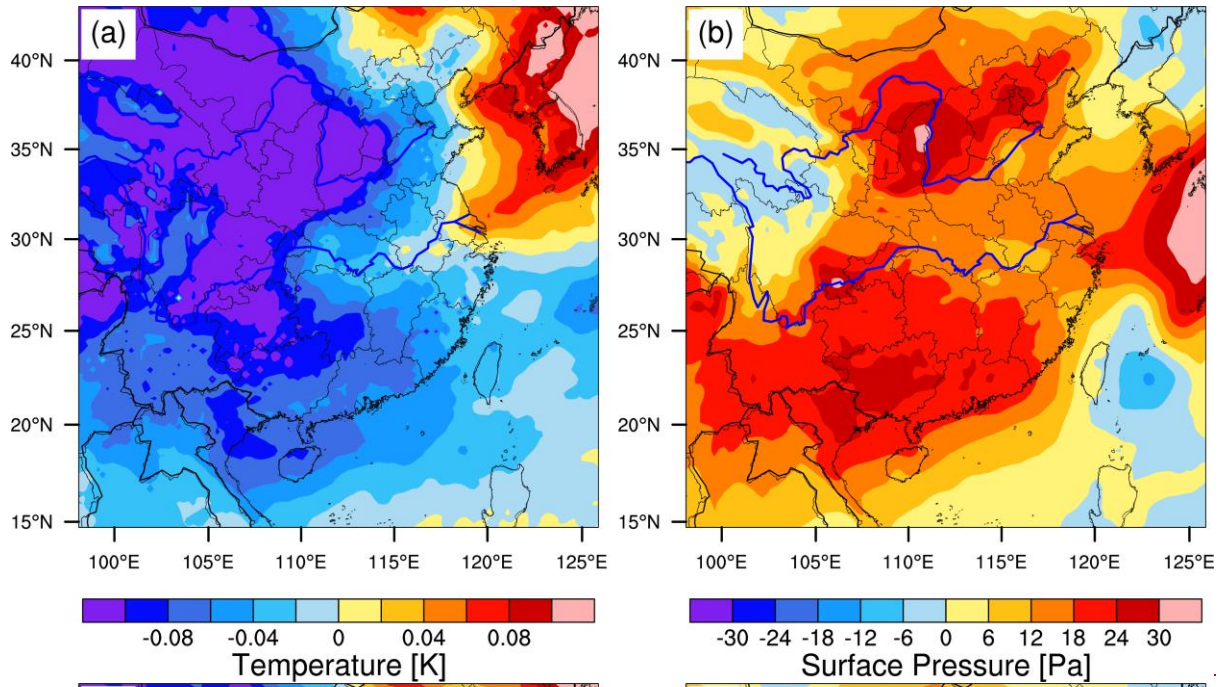


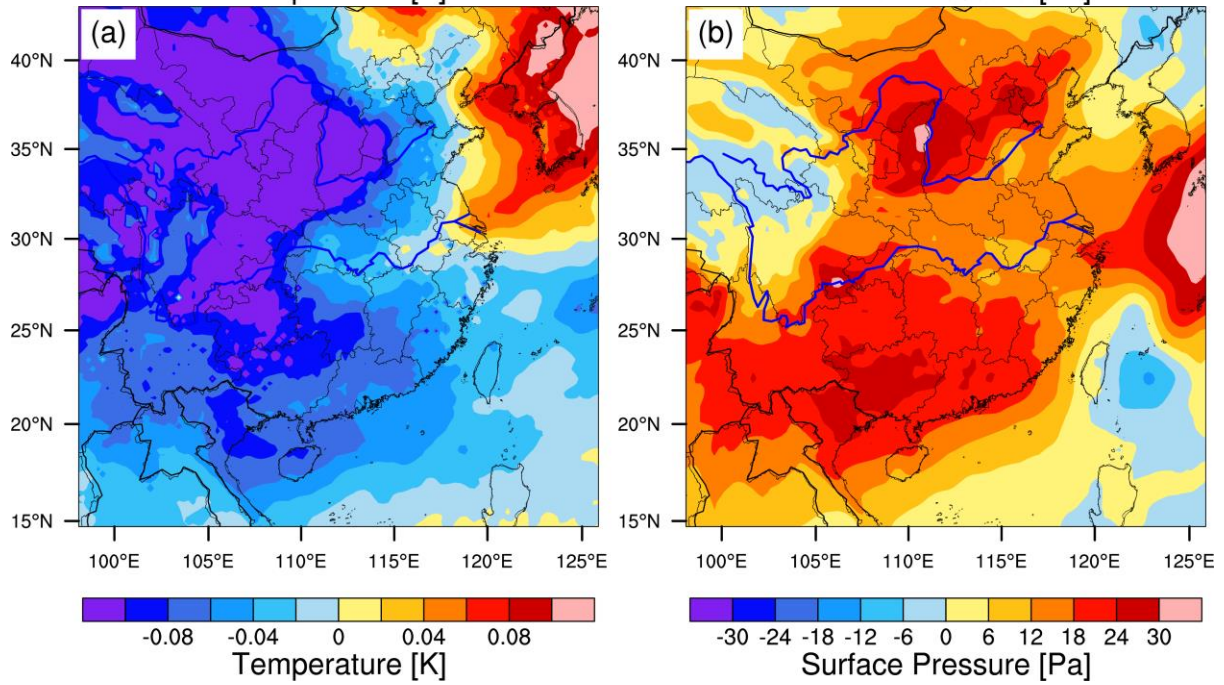
Figure 12. The same as figure 8, but from the large domain simulation.

1406
 1407
 1408
 1409
 1410
 1411
 1412
 1413
 1414
 1415
 1416
 1417
 1418
 1419
 1420
 1421
 1422
 1423
 1424

1425
1426



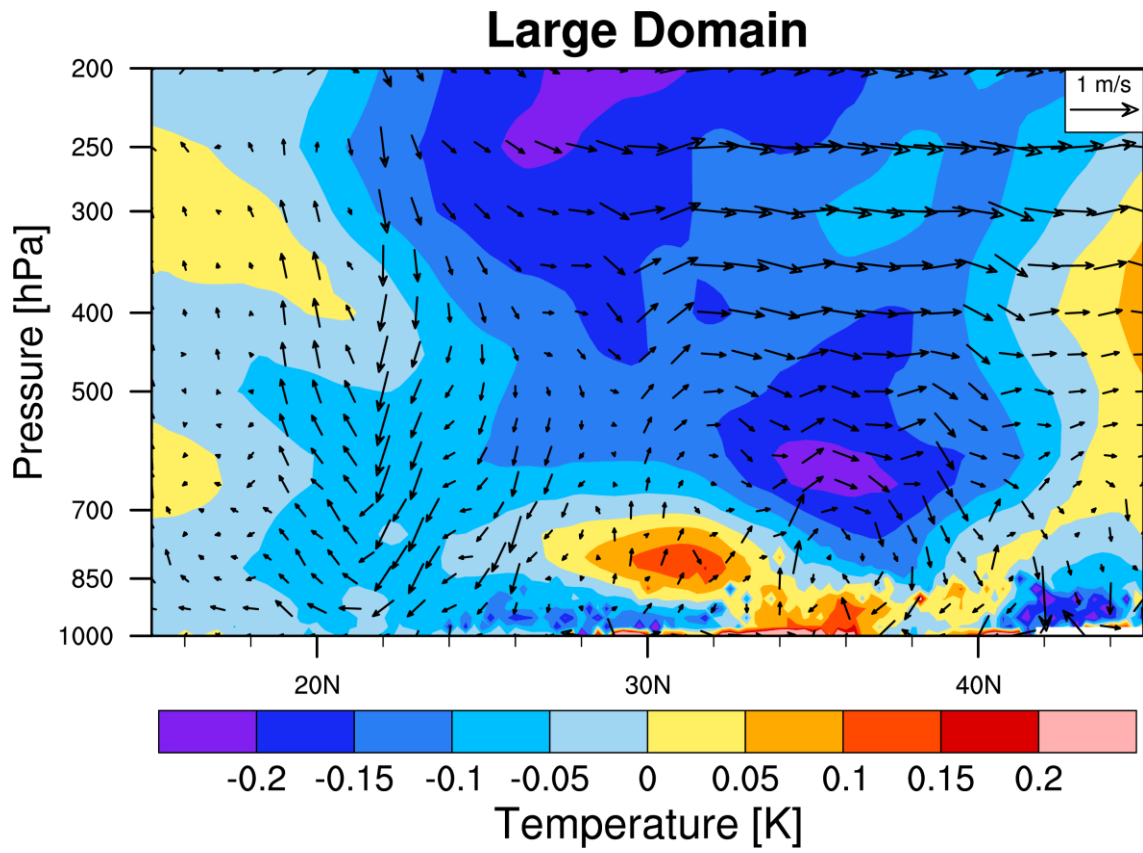
1427



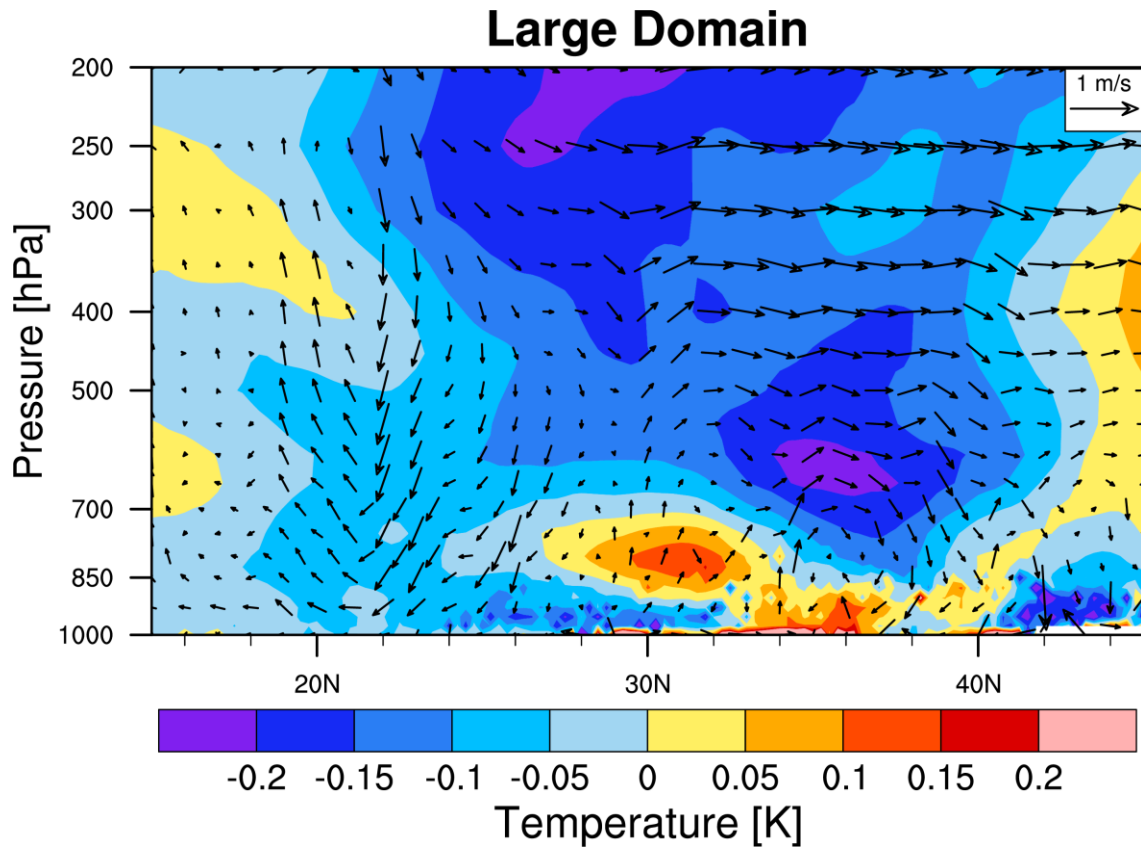
1428
1429
1430
1431
1432
1433
1434
1435
1436
1437

Figure 13. Same as Fig. 9, but from the large domain simulation.

1438
1439
1440
1441
1442
1443
1444
1445
1446
1447
1448
1449
1450
1451
1452
1453
1454

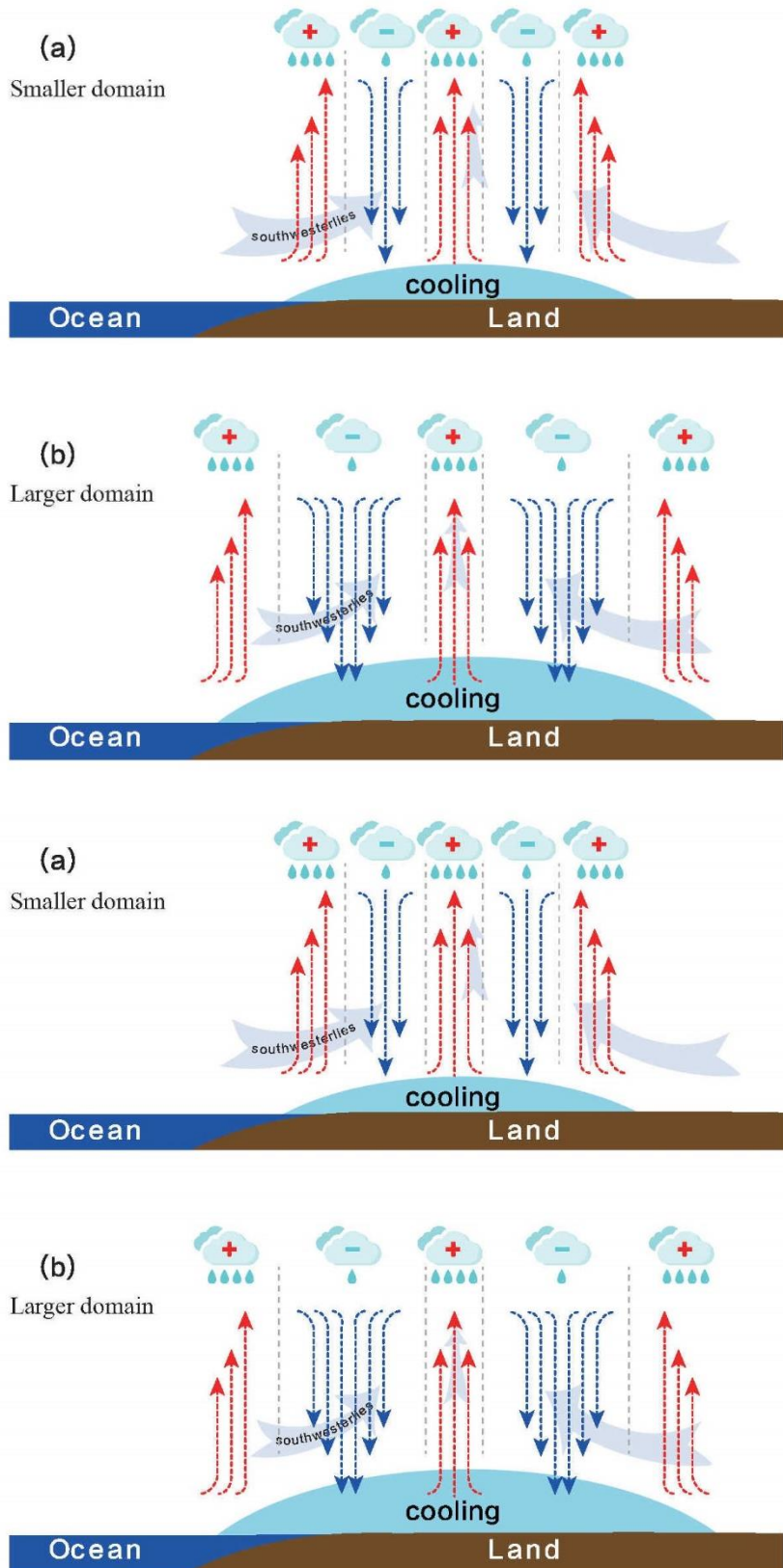


1455



1456
 1457
 1458
 1459
 1460
 1461
 1462
 1463
 1464
 1465
 1466
 1467
 1468
 1469
 1470
 1471
 1472
 1473
 1474
 1475
 1476

Figure 14. Same as figure 11, but from the large domain simulation.



1477

1478

1479

1480

1481

Figure 15. The schematic plot of aerosol ~~impacts~~ impact in (a) small domain simulation and (b) large domain simulation over East Asia. The light blue shadow area represents the extent of aerosol induced decrease of lower tropospheric temperature and increase of surface pressure.

1482 The red (blue) vector dash lines represent updraft (downdraft) anomalies. The “+” (“-”) above
1483 the region indicates the aerosol-induced increase (decrease) of precipitation.
1484